



NRC Publications Archive Archives des publications du CNRC

View planning with positioning system error Scott, William; Roth, Gerhard; Rivest, J.-F.

For the publisher's version, please access the DOI link below. / Pour consulter la version de l'éditeur, utilisez le lien DOI ci-dessous.

<https://doi.org/10.4224/5764906>

NRC Publications Record / Notice d'Archives des publications de CNRC:

<https://nrc-publications.canada.ca/eng/view/object/?id=46c8dd62-826e-448e-aacf-73de867f9561>

<https://publications-cnrc.canada.ca/fra/voir/objet/?id=46c8dd62-826e-448e-aacf-73de867f9561>

Access and use of this website and the material on it are subject to the Terms and Conditions set forth at

<https://nrc-publications.canada.ca/eng/copyright>

READ THESE TERMS AND CONDITIONS CAREFULLY BEFORE USING THIS WEBSITE.

L'accès à ce site Web et l'utilisation de son contenu sont assujettis aux conditions présentées dans le site

<https://publications-cnrc.canada.ca/fra/droits>

LISEZ CES CONDITIONS ATTENTIVEMENT AVANT D'UTILISER CE SITE WEB.

Questions? Contact the NRC Publications Archive team at PublicationsArchive-ArchivesPublications@nrc-cnrc.gc.ca. If you wish to email the authors directly, please see the first page of the publication for their contact information.

Vous avez des questions? Nous pouvons vous aider. Pour communiquer directement avec un auteur, consultez la première page de la revue dans laquelle son article a été publié afin de trouver ses coordonnées. Si vous n'arrivez pas à les repérer, communiquez avec nous à PublicationsArchive-ArchivesPublications@nrc-cnrc.gc.ca.



View Planning with Positioning System Error

William R. Scott^{†‡}, Gerhard Roth[‡], Jean-François Rivest[†]

[†] Department of Electrical Engineering,
University of Ottawa, Ottawa, Canada, K1N 6N5
rivest@site.uottawa.ca

[‡] Computational Video Group,
National Research Council of Canada, Ottawa, Canada, K1A 0R6
(william.scott,gerhard.roth@nrc.ca)

Abstract

Automated 3D object reconstruction or inspection using a range camera requires a positioning system to configure sensor-object relative geometry in a sequence of poses defined by a computed view plan. Discrepancies between commanded and actual poses can result in serious scanning deficiencies. This paper examines the view planning impact of positioning system error on a single view. Counter-measures are suggested to contain data acquisition errors.

1 Introduction

The growing demand for high quality 3D virtual object models has led to a need to automate or semi-automate the model acquisition process. As illustrated at Figure 1, the imaging environment comprises three main elements: object, active range camera [2] and sensor-object positioning system. The model acquisition process typically involves an iterative cycle of view planning, sensing, registration and integration. View planning is the task of determining an optimal set of sensor views or poses. Executing the view plan requires physically altering the sensor-object relative pose by means of a positioning system. Without loss of generality, we can consider the object as fixed and the sensor as mobile. Whenever positioning system accuracy falls below that of the sensor, it is necessary to employ image-based registration¹ to bring images into a common reference frame with a precision comparable to that of surface measurements. The major remaining hurdle to automated model acquisition is achieving an efficient, accurate and robust solution to the view planning component of the data acquisition cycle.

Traditional view planning methods use a variety of non-model-based heuristic techniques relying on surface ([9], [13], [23]), volume ([5], [14], [1], [11], [21], [8])

¹Such as the standard Iterative Closest Point (ICP) algorithm [3] and its more recent enhancements.

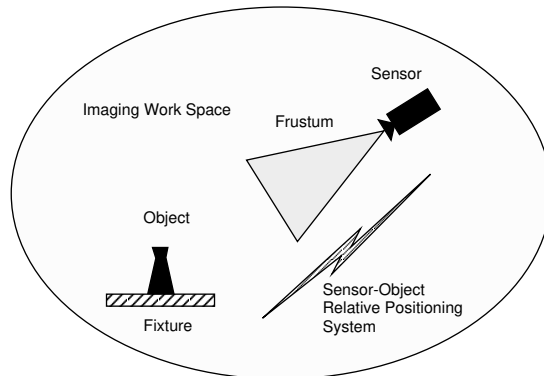


Figure 1: The Geometric Imaging Environment

or global ([24], [12], [7]) scene attributes. A less well-known technique developed by Tarbox and Gottschlich [22] introduced the concept of model-based view planning through the use of measurability matrices. All of these traditional view planning methods have a common attribute. They focus on a single view planning criteria - obtaining complete object coverage. In some cases quality factors are introduced ([8], [22]), but these are subjective in that low grazing angle rays are preferred over high grazing angles rather than evaluating the objective effects of grazing angle on measurement quality.

This work concerns *performance-oriented* reconstruction [15] which is defined as model acquisition based on a set of explicit quality requirements expressed in a *model specification*. In addition to all-aspect coverage, measurement quality is specified in terms of precision, sampling density and perhaps other quality factors. Performance-oriented view planning requires suitable models of both sensor and positioning system performance. Specifically, it requires:

- a *sensor model* to include a description of the frustum and characterization of measurement performance within the calibrated region, and

- a *positioning system model* describing the degrees of freedom, range of motion and positioning accuracy within the movement envelope.

In [18], we described a first-order sensor model suitable for view planning and examined performance trade-offs between the scene exploration and precision measurement phases of view planning.

In this paper, we address the effects on a single planned view of pose error resulting from positioning system inaccuracies. While the focus of the current work is on model building, the analysis is equally applicable to the inspection application. The performance of the positioning system impacts the view planning process, regardless of whether a traditional or performance-oriented view planning algorithm is utilized. For the purposes of this analysis, pose errors are broken down into position error, sensor boresight pointing error (axis error) and rotation error about the sensor boresight (twist error). For each error type, we examine its impact on measurement precision, sampling density, visibility and frustum occupancy. Pose error effects are analyzed in detail for one specific, common sensor configuration, the line-scan range camera. Results are generalizable to other range camera geometries. Input and output parameters in the problem description are normalized and the results quantified, where possible.

An outline of the paper is as follows. We begin in section 2 by defining performance criteria, briefly examine the overall effect of pose error on view planning, provide an overview of positioning systems, define a simple pose error model and define sensor geometry. Section 3 examines in detail the effects of each pose error component on each view planning performance variable. The statistical analysis computes the expected value and variance of each performance variable for each error type. Section 4 concludes with a summary of the results in tabular and graphical form, an analysis of the issues and a discussion of means to mitigate the effects of pose error on view planning.

It is anticipated that the analysis may be beneficial in imaging system design (specifying compatible sensor and positioning system performance) and view planning algorithm design (compensating for positioning system inaccuracy).

2 The View Planning Context

2.1 Performance Criteria

Performance-oriented view planning incorporates two inputs not found in traditional view planning ap-

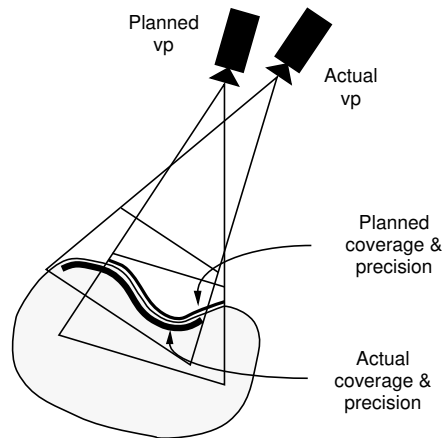


Figure 2: View Planning with Pose Uncertainty

proaches - a model specification and an imaging environment specification. The model specification defines reconstruction goals, such as measurement precision and sampling density, which may be fixed or variable over the object surface. The imaging environment specification defines key sensor and positioning system model parameters.

For a surface point to be declared measurable, all model specification requirements must be met at that surface point for that viewpoint. Specifically, the following tests must be passed:

- *frustum occupancy* - the surface point must fall within the sensor frustum for that viewpoint,
- *visibility* - the surface point must be locally visible from the optical source and receiver positions defined by that viewpoint, and
- *sampling precision and density* - the estimated sampling precision and sampling density at the surface point for that viewpoint must meet the specified requirements.

2.2 Pose Uncertainty Effects

Unfortunately, positioning system errors negatively impact all of these requirements. View planning is a computationally-intensive task with the objective of arriving at a small set of optimal or near-optimal viewpoints, the *next-best-view* (NBV) list. When the NBV list is sent to a positioning system whose position and orientation accuracy is inferior to that of the sensor, the coverage of individual viewpoints and of the NBV list as a whole is compromised. Individual viewpoint positions and orientations are corrupted. Orientation

error is particularly troublesome as effects are amplified by range. As illustrated in Figure 2, *image coverage (frustum occupancy)*, *measurement precision* and *sampling density* will all be effected. *Visibility* can also be effected by the altered viewing geometry.

We can recover a refined pose estimate post-facto by employing suitable registration techniques and subsequently re-estimate measurement quality within the acquired image. However, we are still left with data acquisition differing from that which had been planned. As pose error deteriorates, the computationally intensive view planning phase is progressively compromised - ultimately to be rendered futile. Consequently, there is a need to make the view planning process robust with respect to pose uncertainty resulting from positioning system errors.

Before we can devise compensatory measures, it is necessary to quantify and qualify the various effects. We begin our analysis by presenting a generalized model for positioning system error.

2.3 Positioning Systems

A variety of positioning systems are in common usage, covering a wide range of accuracy. These include co-ordinate measuring machines (CMMs), translation stages, turntables and other rotary joints as well as robot arms and similar devices². At the top end, CMMs offer accuracy superior to the best range camera. At the other extreme, robot arms and similar devices provide good repeatability but comparatively poor accuracy relative to high quality range cameras.

In addition to positioning and orienting the sensor in space, positioning systems are often used to provide one dimension of the sensor scan. For example, a laser scan in the camera x-z plane may be swept along the camera y-axis (line-scan mode) or rotated about an axis parallel to the camera x-axis (cylindrical-scan mode). In such cases, positioning system performance directly effects not only what is scanned (by setting the camera pose) but also the quality of measurement within the range image (by the degree of mechanical jitter). For the present work, we assume that optical and mechanical system components have compatible performance at the image pixel level and restrict our examination to the effects of pose error on overall image coverage and measurement quality.

²A good tutorial on positioning system error mechanisms can be found at [10].

2.4 Positioning System Error Model

In general, it is difficult to characterize the accuracy of positioning systems with multiple degrees of freedom [19], [20], [4]. Accuracy can also be highly variable over the movement envelope for a given machine. For the purposes of analysis, therefore, we adopt the following simplified but general purpose pose error model. First, we assume that calibration has identified, measured and removed from further consideration all systematic error components, leaving only the residual stochastic errors.

Errors in sensor position, boresight axis and rotation about the boresight (twist) are considered to be independent random processes. Position error is modeled as a zero-mean Gaussian process with standard deviation σ_p uniformly distributed in off-set direction. Axis error is modeled by a unit vector uniformly distributed on the surface of a cone centered on the camera boresight where the cone half-angle is a zero-mean Gaussian process with standard deviation σ_a . Twist error is modeled as a zero-mean Gaussian process with standard deviation σ_t . In order to gain an appreciation of the mechanisms involved and their relative importance, we will separately examine each pose error effect in isolation.

While the model just described is a suitable general purpose framework for analyzing the effects of positioning system error, in practice it will be necessary to develop and apply a specific error model tailored to the type, configuration and movement envelope of each unique positioning system in actual usage.

2.5 Range Camera Geometry

To illustrate pose error effects, we examine the case of a line-scan range camera, a common configuration whose imaging geometry is shown at Figure 3. Following the convention in the field, the camera axis defines the negative z-axis. The negative sign is dropped when referring to range along the z-axis, provided the situation is clear. The frustum is defined by Φ_x (the sensor angular field of view in the x-z plane), L_y (the linear scan length in the y-z plane) and R_{min} and R_{max} (the minimum and maximum scanning ranges along the z-axis). The optical transmitter (laser) and optical receiver (detector) are separated by a distance equal to the optical baseline b along the y-axis. In our convention, the origin of the sensor frame of reference is located half way along the linear scan and defines the nominal rest position of the laser. Pose error effects with other imaging configurations depend on the measurement geometry but are similar to those presented here for the line-scan range camera case.

must be separately modeled. However, all share the common characteristic of erosion of the frustum confidence zone.

Field of View Erosion We define a viewpoint's targeted footprint TF as the frustum cross-sectional area at the stand-off range for that viewpoint. The sensor footprint remains unchanged with viewpoint perturbation but pose error will cause it to cover some unplanned regions while losing some planned coverage. The unplanned coverage gain is of no direct benefit in planning a single view while the unplanned coverage loss erodes view planning effectiveness. Thus, for view planning purposes, pose error always reduces and never increases effective coverage.

For a line-scan sensor, the targeted footprint is

$$TF = \underbrace{(2f_d R_o T \Phi_2)}_{width} \underbrace{(L_y)}_{length} \quad (13)$$

where $\Phi_2 = \Phi_x/2$, that is - half the field of view in the x-z plane.

To consider the relative impact of the position component of pose error on effective frustum field of view, it is convenient to define the relative targeted footprint TF_{rel} as

$$TF_{rel} = \frac{TF'}{TF} \quad (14)$$

where TF' is the portion of the sensor footprint disturbed by pose error which overlaps the targeted footprint.

Depth of Field Erosion In considering depth of field, for all practical purposes, only erosion of the effective near-field range limit is of concern. For optimum measurement performance, the stand-off range is set at $z = f_d R_o = f_d R_{min}$. Pose error will result in erosion whenever the z-component of frustum change $\delta_z > (f_d - 1)R_o$. Therefore, the statistic of interest relative to depth of field erosion is the probability $P[\delta_z > (f_d - 1)R_o]$.

3.2 Position Error

The next three sections analyze the effects of each component of pose error on each quality factor as illustrated in Table 1, beginning with pose position error.

As a consequence of changing the location of the entire optical baseline, position error potentially impacts all model specification factors: frustum occupancy, visibility, measurement precision and sampling density.

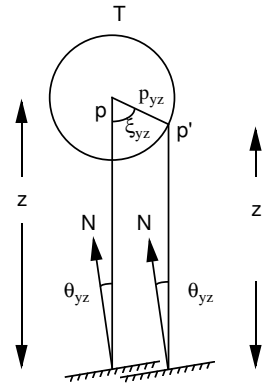


Figure 6: Scanning Geometry Y-Z Plane

3.2.1 Measurement Precision Impact

This section considers the effect of pose position error on measurement precision estimation.

Precision Estimation Model From Equation 4, our model of relative measurement precision is

$$P_{rel} = \frac{z'^2 \cos \theta_{yz}}{z^2 \cos \theta'_{yz}} \quad (15)$$

Assume the viewpoint is optimally positioned at a standoff distance slightly beyond the sensor minimum range i.e. $z = f_d R_o$, $f_d = 1 + \delta$, where $\delta \ll 1$. Sensor position is corrupted by position error $\vec{p} = (p_x, p_y, p_z)$. Then, as shown in Figure 3, z-axis range to the surface element is perturbed to $z' = z + p_z$, that is $z' = f_d R_o + p_z$.

With a line-scan camera subject to pose position error, the inclination angle in the y-z plane with respect to the laser source is unchanged - that is, $\theta_{yz} = \theta_{yz}'$. The scanning geometry is amplified at Figure 6 for clarity. Consequently, P_{rel} simply becomes z'^2/z^2 from which we get

$$\begin{aligned} P_{rel} &= \frac{(f_d R_o + p_z)^2}{(f_d R_o)^2} \\ &= \left(1 + \frac{1}{f_d} \left(\frac{p_z}{R_o}\right)\right)^2 \\ &= 1 + \frac{2}{f_d} \left(\frac{p_z}{R_o}\right) + \frac{1}{f_d^2} \left(\frac{p_z}{R_o}\right)^2. \end{aligned} \quad (16)$$

We wish to estimate the statistics of the relative precision P_{rel} which is a function of the random variable p_z . From our positioning system error model, the expected value and variance of p_z are as follows.

$$\begin{aligned}
E[p_z] &= 0 \\
E[p_z^2] &= \sigma_p^2 \\
&= \sigma_p^2/3.
\end{aligned} \tag{17}$$

Statistics of P_{rel} Consequently,

$$\begin{aligned}
E[P_{rel}] &= \mu_{P_{rel}} \\
&= 1 + \frac{2}{f_d R_o} E[p_z] + \frac{1}{f_d^2 R_o^2} E[p_z^2] \\
&= 1 + \frac{\sigma_p^2}{3f_d^2 R_o^2}.
\end{aligned} \tag{18}$$

To compute the variance of P_{rel} ,

$$\begin{aligned}
E[(P_{rel} - \mu_{P_{rel}})^2] &= \sigma_{P_{rel}}^2 \\
&= E[P_{rel}^2] - (\mu_{P_{rel}})^2.
\end{aligned} \tag{19}$$

Then,

$$E[P_{rel}^2] = E\left[\left(1 + \frac{2}{f_d} \left(\frac{p_z}{R_o}\right) + \frac{1}{f_d^2} \left(\frac{p_z}{R_o}\right)^2\right)^2\right] \tag{20}$$

and, discarding terms over quadratic,

$$\begin{aligned}
E[P_{rel}^2] &\approx E\left[1 + \frac{4}{f_d} \frac{p_z}{R_o} + \frac{6}{f_d^2} \frac{p_z^2}{R_o^2}\right] \\
&= 1 + \frac{2\sigma_p^2}{f_d^2 R_o^2}.
\end{aligned} \tag{21}$$

so, substituting Equations 21 and 16 in Equation 19, we have

$$\sigma_{P_{rel}}^2 = \frac{4}{3f_d^2} \frac{\sigma_p^2}{R_o^2}. \tag{22}$$

Therefore, the relative impact of the position component of pose error on measurement precision estimation is approximately

$$\mu_{P_{rel}} = 1 + \frac{1}{3f_d^2} \frac{\sigma_p^2}{R_o^2}, \tag{23}$$

$$\sigma_{P_{rel}} = \frac{2}{\sqrt{3}f_d} \frac{\sigma_p}{R_o}. \tag{24}$$

Precision Impact Interpretation In Figure 10(a), relative precision P_{rel} computed from Equations 23 and 24 is plotted against normalized position error σ_p/R_o . The latter will typically be very small i.e. $\sigma_p/R_o \ll 1$. Figure 10(a) can be interpreted as follows. One- and two-sigma curves for relative precision are displayed bracketing the nominal value of 1.0. Precision improves for values $P_{rel} < 1$ and deteriorates for values $P_{rel} > 1$. Any vertical slice through these curves defines the shape of the probability density function for relative precision for a given normalized position error. Horizontal lines at $P_{rel} = 1.1$ and $P_{rel} = 0.961$ indicate boundary conditions beyond which measurements will be rejected due to pose position error. The upper limit represents an example of a specified measurement precision limit from the model specification. It has been arbitrarily set at 1.1 in Figure 10(a) for illustration purposes. The lower limit, easily shown to be $1/f_d^2$, defines the point at which measurements are rejected as falling outside the sensor near-range limit. The limit is illustrated here for a value of $f_d = 1.02$, meaning viewpoints are optimized for a standoff distance of 2% beyond the optimal sensor range R_o . The lower limit cut-off is one manifestation of frustum erosion, a topic treated later in more detail.

Examining this error component in isolation, it is apparent from the foregoing that pose position error has a low to moderate impact on measurement precision. The specification clipping effect can be mitigated by selecting suitably conservative model specification limits relative to sensor and positioning system capabilities. Means to mitigate frustum erosion effects will be addressed later.

3.2.2 Sampling Density Impact

Sampling Density Estimation Model This section considers the effect of pose position error on sampling density estimation. From Equation 12, our model for sampling density estimation is

$$D_{rel} = \frac{C^2\theta'_{xz}C^2\theta'_{yz}}{C^2\theta_{xz}C^2\theta_{yz}} \frac{R_{xz}^2C^2\theta_{yz} + f_d^2R_o^2C^2\theta_{xz}}{R'_{xz}{}^2C^2\theta'_{yz} + f_d^2R_o^2C^2\theta'_{xz}}. \tag{25}$$

However, as $\theta'_{yz} = \theta_{yz}$, Equation 25 reduces to

$$D_{rel} = \frac{C^2\theta'_{xz}}{C^2\theta_{xz}} \frac{R_{xz}^2C^2\theta_{yz} + f_d^2R_o^2C^2\theta_{xz}}{R'_{xz}{}^2C^2\theta_{yz} + f_d^2R_o^2C^2\theta'_{xz}}. \tag{26}$$

Key Geometric Parameters We now wish to compute the statistics of D_{rel} which is a function of

the random variables p_{xz} and ξ_{xz} , the magnitude and angle of position error in the scanning plane, respectively. It is useful to first compute simple expressions for the key geometric parameters. From Figure 4, we note that

$$R_{xz}^2 = f_d^2 R_o^2 + x^2 \quad (27)$$

$$R'_{xz}{}^2 = (f_d R_o + p_z)^2 + (x - p_x)^2 \quad (28)$$

and

$$\frac{p_{xz}}{R_{xz}} = \frac{S\delta\theta_{xz}}{S[(\xi_{xz} - \phi_{xz}) + \delta\theta_{xz}]}, \quad (29)$$

Defining $r = p_{xz}/R_{xz} = (p_{xz}C\phi_{xz})/(f_d R_o)$ and setting $\psi_{xz} = \xi_{xz} - \phi_{xz}$, we have the relationship

$$\cot \delta\theta_{xz} = \frac{1 - rC\psi_{xz}}{rS\psi_{xz}} \quad (30)$$

from which we can determine

$$S\delta\theta_{xz} = \frac{rS\psi_{xz}}{\sqrt{1 + r^2 - 2rC\psi_{xz}}}, \quad (31)$$

$$C\delta\theta_{xz} = \frac{1 - rC\psi_{xz}}{\sqrt{1 + r^2 - 2rC\psi_{xz}}}. \quad (32)$$

Noting that $r \ll 1$, the foregoing expressions for $S\delta\theta_{xz}$ and $C\delta\theta_{xz}$ can be written as follows, where we ignore terms in r above quadratic

$$S\delta\theta_{xz} \approx rS\psi_{xz} + r^2 S\psi_{xz} C\psi_{xz}, \quad (33)$$

$$C\delta\theta_{xz} \approx 1 + \frac{r^2}{2}(C^2\psi_{xz} - 1). \quad (34)$$

As an additional precursor to computing the statistics of D_{rel} , we next compute the statistics of ξ_{xz} , r and $\delta\theta_{xz}$. We again only consider terms up to quadratic in r .

Statistics of ξ_{xz}

$$E[S\psi_{xz}] = E[C\psi_{xz}] = E[S\psi_{xz}C\psi_{xz}] = 0 \quad (35)$$

$$E[S^2\psi_{xz}] = E[C^2\psi_{xz}] = 1/2 \quad (36)$$

Statistics of r

$$E[r] = \frac{C\phi_{xz}}{f_d R_o} E[p_{xz}] = 0 \quad (37)$$

$$E[r^2] = \frac{C^2\phi_{xz}}{f_d^2 R_o^2} E[p_{xz}^2] = \frac{2C^2\phi_{xz}}{3f_d^2} \frac{\sigma_p^2}{R_o^2} \quad (38)$$

Statistics of $\delta\theta_{xz}$

$$E[S\delta\theta_{xz}] = E[rS\psi_{xz} + r^2 S\psi_{xz}C\psi_{xz}] = 0 \quad (39)$$

$$\begin{aligned} E[C\delta\theta_{xz}] &= E[1 + \frac{r^2}{2}(C^2\psi_{xz} - 1)] \\ &= 1 - \frac{C^2\phi_{xz}}{6f_d^2} \frac{\sigma_p^2}{R_o^2} \end{aligned} \quad (40)$$

$$\begin{aligned} E[S^2\delta\theta_{xz}] &= E[r^2 S^2\psi_{xz}] \\ &= \frac{C^2\phi_{xz}}{3f_d^2} \frac{\sigma_p^2}{R_o^2} \end{aligned} \quad (41)$$

$$\begin{aligned} E[C^2\delta\theta_{xz}] &= E[1 + r^2(C^2\psi_{xz} - 1)] \\ &= 1 - \frac{C^2\phi_{xz}}{3f_d^2} \frac{\sigma_p^2}{R_o^2} \end{aligned} \quad (42)$$

$$E[S\delta\theta_{xz}C\delta\theta_{xz}] = E[rS\psi_{xz} + r^2 S\psi_{xz}C\psi_{xz}] = 0 \quad (43)$$

Simplification of D_{rel} We now have most of the ingredients to calculate the statistics of the relative sampling density D_{rel} . First, it is convenient to rewrite Equation 26 as the product of a constant term T1 and a variable term T2.

$$D_{rel} = \underbrace{\frac{R_{xz}^2}{f_d^2 R_o^2} C^2\theta_{yz} + C^2\theta_{xz}}_{T1} \underbrace{\frac{C^2\theta'_{xz}}{\frac{(R'_{xz})^2}{f_d^2 R_o^2} C^2\theta_{yz} + C^2\theta'_{xz}}}_{T2} \quad (44)$$

Consider T1. As $R_{xz}/(f_d R_o) = 1/C\phi_{xz}$, T1 reduces to

$$T1 = \frac{C^2\theta_{yz} + C^2\phi_{xz}C^2\theta_{xz}}{C^2\phi_{xz}C^2\theta_{xz}}. \quad (45)$$

Let $T2 = N2/D2$. Then,

$$D2 = \frac{R'_{xz}{}^2}{f_d^2 R_o^2} C^2\theta_{yz} + C^2\theta'_{xz}. \quad (46)$$

Considering the first term in 46 and using Equation 28, we have

$$\begin{aligned} \frac{R'_{xz}{}^2}{f_d^2 R_o^2} &= 1 + \frac{2}{f_d} \frac{p_z}{R_o} + \frac{1}{f_d^2} \frac{p_z^2}{R_o^2} + T^2\phi_{xz} \\ &\quad - \frac{2T\phi_{xz}p_x}{f_d R_o} + \frac{1}{f_d^2} \frac{p_x^2}{R_o^2} \\ &= \frac{1}{C^2\phi_{xz}}(1 + t_r) \end{aligned} \quad (47)$$

where t_r is

$$t_r = \frac{2C^2\phi_{xz} p_z}{f_d R_o} + \frac{C^2\phi_{xz} p_z^2}{f_d^2 R_o^2} - \frac{2S\phi_{xz}C\phi_{xz} p_x}{f_d R_o} + \frac{C^2\phi_{xz} p_x^2}{f_d^2 R_o^2}. \quad (48)$$

Considering the term $C^2\theta'_{xz}$ in 46

$$\begin{aligned} C^2\theta'_{xz} &= C^2(\theta_{xz} + \delta\theta_{xz}) \\ &= (C\theta_{xz}C\delta\theta_{xz} - S\theta_{xz}S\delta\theta_{xz})^2 \\ &= C^2\theta_{xz}C^2\delta\theta_{xz} - 2S\theta_{xz}C\theta_{xz}S\delta\theta_{xz}C\delta\theta_{xz} \\ &\quad + S^2\theta_{xz}S^2\delta\theta_{xz}. \end{aligned} \quad (49)$$

Then, using the relationships from 33 and 34,

$$S^2\delta\theta_{xz} \approx r^2 S^2\psi_{xz} \quad (50)$$

$$C^2\delta\theta_{xz} \approx 1 + r^2(C^2\psi_{xz} - 1) \quad (51)$$

$$S\delta\theta_{xz}C\delta\theta_{xz} \approx rS\psi_{xz} + r^2S\psi_{xz}C\psi_{xz} \quad (52)$$

so that we have

$$\begin{aligned} C^2\theta'_{xz} &\approx C^2\theta_{xz}[1 + r^2(C^2\psi_{xz} - 1)] \\ &\quad - 2S\theta_{xz}C\theta_{xz}[rS\psi_{xz} + r^2S\psi_{xz}C\psi_{xz}] \\ &\quad + S^2\theta_{xz}r^2S^2\psi_{xz} \\ &= C^2\theta_{xz}[1 + t_\theta] \end{aligned} \quad (53)$$

where

$$t_\theta = -2rT\theta_{xz}S\psi_{xz} + r^2(C^2\psi_{xz} - 1) - 2r^2T\theta_{xz}S\psi_{xz}C\psi_{xz} + r^2T^2\theta_{xz}S^2\psi_{xz}. \quad (54)$$

Now, combining the expressions for $R'_{xz}/(f_d^2 R_o^2)$ and $C^2\theta'_{xz}$ with Equation 46, we have

$$\begin{aligned} D2 &= \frac{R'_{xz}}{f_d^2 R_o^2} C^2\theta_{yz} + C^2\theta'_{xz} \\ &= \frac{C^2\theta_{yz}}{C^2\phi_{xz}} [1 + t_r] + C^2\theta_{xz} [1 + t_\theta] \\ &= \frac{C^2\theta_{yz} + C^2\theta_{xz}C^2\phi_{xz}}{C^2\phi_{xz}} [1 \\ &\quad + \frac{C^2\theta_{yz}}{C^2\theta_{yz} + C^2\theta_{xz}C^2\phi_{xz}} t_r \end{aligned}$$

$$\begin{aligned} &+ \frac{C^2\theta_{xz}C^2\phi_{xz}}{C^2\theta_{yz} + C^2\theta_{xz}C^2\phi_{xz}} t_\theta] \\ &= \frac{C^2\theta_{yz} + C^2\theta_{xz}C^2\phi_{xz}}{C^2\phi_{xz}} [1 + t] \end{aligned} \quad (55)$$

where

$$\begin{aligned} t &= \frac{C^2\theta_{yz}}{C^2\theta_{yz} + C^2\theta_{xz}C^2\phi_{xz}} t_r \\ &\quad + \frac{C^2\theta_{xz}C^2\phi_{xz}}{C^2\theta_{yz} + C^2\theta_{xz}C^2\phi_{xz}} t_\theta. \end{aligned} \quad (56)$$

Now, the expression for T2 from Equation 46 can be simplified to

$$T2 = \frac{C^2\theta_{xz}C^2\phi_{xz}}{C^2\theta_{yz} + C^2\theta_{xz}C^2\phi_{xz}} \frac{[1 + t_\theta]}{[1 + t]}. \quad (57)$$

Statistics of D_{rel} Finally, combining 45 and 57, we have the following expression for D_{rel} :

$$D_{rel} = \frac{[1 + t_\theta]}{[1 + t]}. \quad (58)$$

As $|t| < 1$, the denominator of 58 can be expressed as a series expansion. After expansion and collecting terms up to quadratic in t_θ and t , we have the following second order approximations for D_{rel} and D_{rel}^2 :

$$D_{rel} \approx 1 - t + t^2 + t_\theta - tt_\theta, \quad (59)$$

$$D_{rel}^2 \approx 1 - 2t + 3t^2 + 2t_\theta - 4tt_\theta + t_\theta^2. \quad (60)$$

Using the interim results previously developed, the statistics of terms in t_θ and t can be expressed as follows:

$$E[t_\theta] = \frac{C^2\phi_{xz} \sigma_p^2}{3f_d^2 R_o^2} (T^2\theta_{xz} - 1) \quad (61)$$

$$E[t_\theta^2] = \frac{4T^2\theta_{xz}C^2\phi_{xz} \sigma_p^2}{3f_d^2 R_o^2} \quad (62)$$

$$E[t_r] = \frac{2C^2\phi_{xz} \sigma_p^2}{3f_d^2 R_o^2} \quad (63)$$

$$E[t_r^2] = \frac{8C^2\phi_{xz} \sigma_p^2}{3f_d^2 R_o^2} \quad (64)$$

$$E[t] = \frac{C^2\phi_{xz} \sigma_p^2}{3f_d^2 R_o^2} \frac{[2C^2\theta_{yz} + C^2\phi_{xz}(S^2\theta_{xz} - C^2\theta_{xz})]}{C^2\theta_{yz} + C^2\theta_{xz}C^2\phi_{xz}} \quad (65)$$

$$E[t^2] = \frac{4C^2\phi_{xz} \sigma_p^2}{3f_d^2 R_o^2} \frac{[2C^4\theta_{yz} + C^4\phi_{xz}S^2\theta_{xz}C^2\theta_{xz}]}{(C^2\theta_{yz} + C^2\theta_{xz}C^2\phi_{xz})^2} \quad (66)$$

$$E[t_\theta t_r] = 0 \quad (67)$$

$$E[tt_\theta] = \frac{4S^2\theta_{xz}C^4\phi_{xz} \sigma_p^2}{3f_d^2 R_o^2} \frac{1}{[C^2\theta_{yz} + C^2\theta_{xz}C^2\phi_{xz}]} \quad (68)$$

After these laborious calculations, we can finally express the statistics of D_{rel} from 59 and 60 as follows after collecting terms up to quadratic in σ_p/R_o and simplifying:

$$\begin{aligned} E[D_{rel}] &= \mu_{D_{rel}} \\ &= 1 + \frac{C^2\theta_{yz}C^2\phi_{xz} \sigma_p^2}{3C^2\theta_{xz}f_d^2 R_o^2} \\ &\quad \frac{4C^2\theta_{xz}C^2\theta_{yz} - 3C^2\theta_{xz}C^2\phi_{xz} + C^2\theta_{yz}}{(C^2\theta_{yz} + C^2\theta_{xz}C^2\phi_{xz})^2} \end{aligned} \quad (69)$$

$$\begin{aligned} E[D_{rel}^2] &= 1 + \frac{2C^2\theta_{yz}C^2\phi_{xz} \sigma_p^2}{C^2\theta_{xz}f_d^2 R_o^2} \\ &\quad \frac{2C^2\theta_{xz}C^2\theta_{yz} - C^2\theta_{xz}C^2\phi_{xz} + C^2\theta_{yz}}{(C^2\theta_{yz} + C^2\theta_{xz}C^2\phi_{xz})^2} \end{aligned} \quad (70)$$

so the variance and standard deviation of D_{rel} are

$$\sigma_{D_{rel}}^2 = \frac{4C^4\theta_{yz}C^2\phi_{xz}(C^2\phi_{xz} + 1)}{3C^2\theta_{xz}f_d^2(C^2\theta_{yz} + C^2\theta_{xz}C^2\phi_{xz})^2} \frac{\sigma_p^2}{R_o^2}, \quad (71)$$

$$\sigma_{D_{rel}} = \frac{2C^2\theta_{yz}C\phi_{xz}\sqrt{C^2\phi_{xz} + 1}}{\sqrt{3}C\theta_{xz}f_d(C^2\theta_{yz} + C^2\theta_{xz}C^2\phi_{xz})} \frac{\sigma_p}{R_o}. \quad (72)$$

In summary, the relative impact of pose position error on sampling density estimation is approximately

$$\mu_{D_{rel}}$$

$$\begin{aligned} &= 1 + \frac{C^2\theta_{yz}C^2\phi_{xz} \sigma_p^2}{3C^2\theta_{xz}f_d^2 R_o^2} \\ &\quad \frac{4C^2\theta_{xz}C^2\theta_{yz} - 3C^2\theta_{xz}C^2\phi_{xz} + C^2\theta_{yz}}{(C^2\theta_{yz} + C^2\theta_{xz}C^2\phi_{xz})^2}, \end{aligned} \quad (73)$$

$$\sigma_{D_{rel}} = \frac{2C^2\theta_{yz}C\phi_{xz}\sqrt{C^2\phi_{xz} + 1}}{\sqrt{3}C\theta_{xz}f_d(C^2\theta_{yz} + C^2\theta_{xz}C^2\phi_{xz})} \frac{\sigma_p}{R_o}. \quad (74)$$

For an optimum scanning geometry such that $\phi_{xz} = \theta_{xz} = \theta_{yz} = 0$, the statistics of relative sampling density D_{rel} reduce to the following:

$$\mu_{D_{rel}} = 1 + \frac{1}{3f_d^2} \frac{\sigma_p^2}{R_o^2}, \quad (75)$$

$$\sigma_{D_{rel}} = \frac{\sqrt{2}}{\sqrt{3}f_d} \frac{\sigma_p}{R_o}. \quad (76)$$

Sampling Density Impact Interpretation The impact of pose position error on sampling density estimation calculated at Equations 75 and 76 is shown in Figure 10(c) for the optimum scanning geometry. Sampling density improves for values $D_{rel} > 1$ and deteriorates for values $D_{rel} < 1$. The effects will be seen to very close to those for measurement precision as shown at Figure 10(a) and can be interpreted in a similar manner. As was the case for measurement precision, it is apparent from the foregoing that pose position error has a low to moderate impact on sampling density.

3.2.3 Visibility Impact

Visibility or occlusion effects depend on object shape, optical baseline length and sensor-object relative pose. The optical baseline is fixed and camera pose has been optimized in the viewpoint generation process. Relative visibility effects therefore depend mainly on object geometry. They cannot be quantified in the absence of a specific object shape. However, from the previous analysis, we can observe that the visibility impact of pose position error will be nil to low. This is due to the very small changes in observation geometry between surface points, laser source and optical receiver as a consequence of the low normalized position error σ_p/R_o anticipated for most imaging environments.

3.2.4 Frustum Occupancy Impact

This section considers the effect of pose position error on frustum occupancy.

Frustum Erosion From Equation 13, the targeted footprint is

$$TF = \underbrace{(2f_d R_o T \Phi_2)}_{width} \underbrace{(L_y)}_{length}. \quad (77)$$

Pose error $\vec{p} = (p_x, p_y, p_z)$ erodes coverage as follows. p_x reduces the width by $|p_x|$, p_y reduces the length by $|p_y|$ while p_z reduces the width by $T\Phi_2|p_z|$. The later relationship can be seen from the following. For $p_z < 0$, width is reduced by $2T\Phi_2|p_z|$. For $p_z > 0$, width is increased by $2T\Phi_2|p_z|$. However, the increase for $p_z > 0$ is of no benefit. The net effect of z-axis pose error is a coverage reduction of $T\Phi_2|p_z|$. Consequently, the portion of the targeted footprint covered by the viewpoint subject to pose position error is

$$TF' = (2f_d R_o T \Phi_2 - T\Phi_2|p_z| - |p_x|)(L_y - |p_y|). \quad (78)$$

Then, the TF_{rel} is

$$\begin{aligned} TF_{rel} &= \frac{TF'}{TF} \\ &= \frac{(2f_d R_o T \Phi_2 - T\Phi_2|p_z| - |p_x|)(L_y - |p_y|)}{2f_d R_o T \Phi_2 L_y}. \end{aligned} \quad (79)$$

As before, we optimize the viewpoint by setting $L_y = f_d R_o \Phi_x$ which gives us

$$TF_{rel} = \frac{(2f_d R_o T \Phi_2 - T\Phi_2|p_z| - |p_x|)(f_d R_o \Phi_x - |p_y|)}{2f_d R_o T \Phi_2 f_d R_o \Phi_x}. \quad (80)$$

We now wish to compute the statistics of TF_{rel} which is a function of the random variables p_x, p_y, p_z . First, we need the statistics of $|p_x|, |p_y|, |p_z|$. It is readily shown that

$$E[|p_x|] = \sigma_p \sqrt{\frac{2}{3\pi}}, \quad (81)$$

$$E[|p_x|^2] = \frac{\sigma_p^2}{3}, \quad (82)$$

$$E[|p_x||p_y|] = \frac{2\sigma_p^2}{3\pi}. \quad (83)$$

Given our model of pose error, the statistics of p_x, p_y and p_z are identical. Therefore, 80 can be written as

$$TF_{rel} = 1 - a|p_x| + b|p_x||p_y| \quad (84)$$

where

$$a = \frac{(\Phi_x T \Phi_2 + \Phi_x + 2T \Phi_2)}{2f_d R_o \Phi_x T \Phi_2} \quad (85)$$

and

$$b = \frac{(T \Phi_2 + 1)}{2f_d^2 R_o^2 \Phi_x T \Phi_2}. \quad (86)$$

Thus,

$$\begin{aligned} E[TF_{rel}] &= \mu_{TF_{rel}} \\ &= 1 - a\sigma_p \sqrt{\frac{2}{3\pi}} + \frac{2b\sigma_p^2}{3\pi}. \end{aligned} \quad (87)$$

Considering only terms up to quadratic

$$\mu_{TF_{rel}}^2 \approx 1 + \frac{2a^2\sigma_p^2}{3\pi} - 2a\sigma_p \sqrt{\frac{2}{3\pi}} + \frac{4b\sigma_p^2}{3\pi} \quad (88)$$

and from Equation 84

$$TF_{rel}^2 \approx 1 + a^2|p_x|^2 - 2a|p_x| + 2b|p_x||p_y|, \quad (89)$$

$$E[TF_{rel}^2] = 1 + \frac{a^2\sigma_p^2}{3} - 2a\sigma_p \sqrt{\frac{2}{3\pi}} + \frac{4b\sigma_p^2}{3\pi}. \quad (90)$$

Therefore,

$$\begin{aligned} \sigma_{TF_{rel}}^2 &= E[TF_{rel}^2] - \mu_{TF_{rel}}^2 \\ &= \frac{a^2\sigma_p^2(\pi - 2)}{3\pi}. \end{aligned} \quad (91)$$

In summary, the relative impact of pose position error on field of view erosion is approximately

$$\begin{aligned} \mu_{TF_{rel}} &= 1 - \frac{(\Phi_x T \Phi_2 + \Phi_x + 2T \Phi_2)}{2f_d \Phi_x T \Phi_2} \sqrt{\frac{2}{3\pi}} \frac{\sigma_p}{R_o} \\ &\quad + \frac{(T \Phi_2 + 1)}{3\pi f_d^2 \Phi_x T \Phi_2 R_o^2} \sigma_p^2, \end{aligned} \quad (92)$$

$$\sigma TF_{rel} = \frac{(\Phi_x T\Phi_2 + \Phi_x + 2T\Phi_2)}{2f_d\Phi_x T\Phi_2} \sqrt{\frac{\pi-2}{3\pi}} \frac{\sigma_p}{R_o}. \quad (93)$$

The impact of pose position error on viewpoint coverage calculated from Equations 92 and 93 is shown at Figure 10(e) for a line-scan sensor with $\Phi_x = 30^\circ$, $f_d = 1.02$ and the optimum scanning geometry. Viewpoint coverage and effective field of view deteriorates for $TF_{rel} < 1$. By definition, TF_{rel} never exceeds one. One- and two-sigma curves for relative targeted footprint are displayed bracketing the average value. We observe that there is moderate frustum erosion with pose position error. Hence, it is an important factor in view planning.

Depth of Field Erosion As previously noted, pose error will result in erosion whenever $\delta_z > (f_d - 1)R_o$. With pose position error, such an event is catastrophic as the entire scan is compromised at the targeted standoff distance. Therefore, the only statistic of interest relative to depth of field erosion is the probability $P[p_z > (f_d - 1)R_o]$. Then,

$$P[p_z > \epsilon] = 1 - \Phi\left[\frac{\epsilon - \mu}{\sigma_z}\right] \quad (94)$$

where $\sigma_z = \sigma_p/\sqrt{3}$, $\mu = 0$, $\epsilon = (f_d - 1)R_o$ and

$$\Phi[z] = \frac{1}{\sqrt{2\pi}} \int_{-\infty}^z e^{-u^2/2} du. \quad (95)$$

Then

$$P[p_z > (f_d - 1)R_o] = 1 - \Phi\left[\frac{\sqrt{3}(f_d - 1)}{(\sigma_p/R_o)}\right]. \quad (96)$$

The probability of depth of field erosion with pose position error is shown at Figure 10(b), plotted on a normalized logarithmic scale. These curves can be used to select a suitable distance factor f_d for a given level of pose error and tolerance for depth of field erosion.

3.3 Axis Error

3.3.1 Measurement Precision Impact

Precision Estimation Model This section considers the effect of the axis component of pose orientation error on measurement precision estimation. For the line-scan range camera examined here, we follow the convention that the frustum origin (which coincides with the laser rest position) falls half way along the y-axis linear scan (Figure 3). The sensor boresight

is defined by the sensor negative z-axis. Axis error is modeled by a unit vector uniformly distributed on the surface of a cone centered on the camera boresight. Effectively, axis error involves rotations about the sensor x and y axes. These can be combined into a single rotation of angle α about an axis \vec{r} in the xy-plane at angle β . The axis error cone half-angle α is modeled as a zero-mean Gaussian process with standard deviation σ_a while β , the angle in the xy-plane at which the axis error occurs, has a uniform distribution over $[-\pi, \pi]$.

The corresponding rotation matrix $R_{r,\alpha}$ is as follows [6], where $V\alpha$ is $vers\ \alpha = 1 - \cos\ \alpha$:

$$\begin{pmatrix} r_x^2 V\alpha + C\alpha & r_x r_y V\alpha - r_z S\alpha & r_x r_z V\alpha + r_y S\alpha \\ r_x r_y V\alpha + r_z S\alpha & r_y^2 V\alpha + C\alpha & r_y r_z V\alpha - r_x S\alpha \\ r_x r_z V\alpha - r_y S\alpha & r_y r_z V\alpha + r_x S\alpha & r_z^2 V\alpha + C\alpha \end{pmatrix} \quad (97)$$

As the rotation vector \vec{r} lies in the xy-plane, $\vec{r} = (r_x, r_y, r_z) = (S\beta, C\beta, 0)$. We can therefore simplify 97 to

$$R_{r,\alpha} = \begin{pmatrix} S^2\beta V\alpha + C\alpha & S\beta C\beta V\alpha & C\beta S\alpha \\ S\beta C\beta V\alpha & C^2\beta V\alpha + C\alpha & -S\beta S\alpha \\ -C\beta S\alpha & S\beta S\alpha & C\alpha \end{pmatrix} \quad (98)$$

It is again convenient to deal with relative precision P_{rel} from 4

$$P_{rel} = \frac{z'^2 \cos\ \theta_{yz}}{z^2 \cos\ \theta'_{yz}}. \quad (99)$$

We assume the sensor range has been optimally set at $z = f_d R_o$. From 98,

$$z' = -C\beta S\alpha x + S\beta S\alpha y + C\alpha z. \quad (100)$$

Inclination angle θ_{yz} is the angle between the projection of the surface normal \vec{n} on the y-z plane in camera space in the absence of pose axis error - that is, $\vec{n}_{yz} = (0, n_y, n_z)$, and the negative of the camera boresight $\vec{u}_z = (0, 0, 1)$. Similarly, inclination angle θ'_{yz} is the angle between the surface normal in camera space in the y-z plane in the presence of pose axis error $\vec{n}_{yz}' = (0, n_y', n_z')$ and $\vec{u}_z' = (0, 0, 1)$.

Here,

$$\begin{aligned} n_y' &= S\beta C\beta V\alpha n_x + (C^2\beta V\alpha + C\alpha)n_y - S\beta S\alpha n_z, \\ n_z' &= C\beta S\beta n_x + S\beta S\alpha n_y + C\alpha n_z. \end{aligned} \quad (101)$$

Then,

$$C\theta_{yz} = \frac{\vec{n}_{yz} \cdot \vec{u}_z}{\|\vec{n}_{yz}\| \|\vec{u}_z\|}, \quad (102)$$

$$C\theta'_{yz} = \frac{\vec{n}_{yz}' \cdot \vec{u}_z'}{\|\vec{n}_{yz}'\| \|\vec{u}_z'\|}. \quad (103)$$

Let us consider the case where the sensor is optimally positioned such that the inclination angles are zero. Therefore, $\theta_{xz} = \theta_{yz} = 0$ which implies $\vec{n} = (0, 0, 1)$. Additionally, we are concerned only with points near the sensor boresight - that is, $x = y = 0$. Then, $\vec{n}_{yz}' = (0, -S\beta S\alpha, C\alpha)$, $z'^2/z^2 = C^2\alpha$ and

$$C\theta_{yz} = 1, \quad (104)$$

$$C\theta'_{yz} = \frac{C\alpha}{\sqrt{S^2\beta S^2\alpha + C^2\alpha}}. \quad (105)$$

Then, the expression for relative precision P_{rel} at Equation 99 is

$$\begin{aligned} P_{rel} &= C^2\alpha \frac{\sqrt{S^2\beta S^2\alpha + C^2\alpha}}{C\alpha} \\ &= C^2\alpha \sqrt{S^2\beta T^2\alpha + 1}. \end{aligned} \quad (106)$$

As $T^2\alpha \ll 1$, 106 can be written as follows

$$\begin{aligned} P_{rel} &= C^2\alpha \left(1 + \frac{S^2\beta T^2\alpha}{2} - \frac{S^4\beta T^4\alpha}{8}\right) \\ &= C^2\alpha + \frac{S^2\beta S^2\alpha}{2} - \frac{S^4\beta T^2\alpha S^2\alpha}{8}. \end{aligned} \quad (107)$$

As a precursor to computing the statistics of P_{rel} , we next compute the statistics of α and β .

Statistics of β Recalling that β has a uniform distribution over $[-\pi, \pi]$, it can be shown that

$$E[S\beta] = E[C\beta] = E[S\beta C\beta] = 0 \quad (108)$$

$$E[S^2\beta] = E[C^2\beta] = 1/2 \quad (109)$$

$$E[S\beta C^2\beta] = E[S^2\beta C\beta] = E[S^3\beta] = 0 \quad (110)$$

$$E[S^2\beta C^2\beta] = 1/8 \quad (111)$$

$$E[S^4\beta] = 3/8 \quad (112)$$

$$E[|S\beta|] = E[|C\beta|] = 2/\pi \quad (113)$$

$$E[|S\beta C\beta|] = 1/\pi \quad (114)$$

Statistics of α As α is a zero-mean Gaussian process with standard deviation σ_a , it can be shown that

$$E[S\alpha] = 0 \quad (115)$$

$$E[C\alpha] = e^{(-\frac{\sigma_a^2}{2})} \approx 1 - \frac{\sigma_a^2}{2} \quad (116)$$

$$E[T^2\alpha] = E[S^2\alpha] \approx \sigma_a^2 \quad (117)$$

$$E[C^2\alpha] \approx 1 - \sigma_a^2 \quad (118)$$

$$E[C^4\alpha] \approx 1 - 2\sigma_a^2 \quad (119)$$

$$E[S\alpha T\alpha] \approx \sigma_a^2 \quad (120)$$

$$E[S\alpha T^2\alpha] = 0 \quad (121)$$

$$E[S\alpha T^3\alpha] = E[S^2\alpha T^2\alpha] = \mathcal{O}(\sigma_a^4) \quad (122)$$

$$E[|T\alpha|] = \sigma_a \sqrt{\frac{2}{\pi}} \quad (123)$$

$$E[S\alpha C\alpha] = 0 \quad (124)$$

$$E[S^2\alpha C^2\alpha] = \sigma_a^2 \quad (125)$$

Statistics of P_{rel} With the above results, we can now compute the statistics of P_{rel} . Applying the expected value operator to 107 and retaining terms up to quadratic in σ_a , we get the following approximation

$$\mu_{P_{rel}} = 1 - \frac{3\sigma_a^2}{4}. \quad (126)$$

Similarly, to compute the variance

$$(\mu_{P_{rel}})^2 \approx 1 - \frac{3\sigma_a^2}{2}, \quad (127)$$

$$\begin{aligned} \mu_{P_{rel}^2} &= E[C^4\alpha + S^2\beta S^2\alpha C^2\alpha] \\ &= 1 - \frac{3\sigma_a^2}{2}. \end{aligned} \quad (128)$$

So, using terms up to quadratic in σ_a , the variance $\sigma_{P_{rel}^2}$ is

$$\begin{aligned} \sigma_{P_{rel}^2} &= \mu_{P_{rel}^2} - (\mu_{P_{rel}})^2 \\ &= 0. \end{aligned} \quad (129)$$

Precision Impact Interpretation In summary, for the optimal viewing geometry (zero inclination angle and measurements near the sensor boresight), $\mu_{P_{rel}}$ and $\sigma_{P_{rel}}^2$ are as follows. Average precision is marginally improved while the variance is zero. The first effect results from the small but consistent range reduction with axis error, while the second is due to the symmetrical viewing geometry under these conditions.

$$\mu_{P_{rel}} = 1 - \frac{3\sigma_a^2}{4}, \quad (130)$$

$$\sigma_{P_{rel}}^2 = 0. \quad (131)$$

3.3.2 Sampling Density Impact

Sampling Density Estimation Model This section considers the effect of the axis component of pose orientation error on sampling density estimation. From Equation 12, our model for relative sampling density D_{rel} is

$$D_{rel} = \frac{C^2\theta'_{xz}C^2\theta'_{yz} R_{xz}^2C^2\theta_{yz} + f_d^2R_o^2C^2\theta_{xz}}{C^2\theta_{xz}C^2\theta_{yz} R'_{xz}{}^2C^2\theta'_{yz} + f_d^2R_o^2C^2\theta'_{xz}}. \quad (132)$$

For axis error angle α at angle β to the xy-plane co-ordinate frame, we have the following geometric relationships:

$$R_{xz}^2 = z^2 + x^2 = f_d^2R_o^2 + x^2, \quad (133)$$

$$R'_{xz}{}^2 = z'^2 + x'^2, \quad (134)$$

$$z' = -C\beta S\alpha x + S\beta S\alpha y + C\alpha z, \quad (135)$$

$$x' = (S^2\beta V\alpha + C\alpha)x + S\beta C\alpha V\alpha y + C\beta S\alpha z. \quad (136)$$

With the sensor in the optimal scanning configuration, $\theta_{xz} = \theta_{yz} = 0$ and $x = y = 0$. Then, as shown in the previous section

$$x' = C\beta S\alpha f_d R_o, \quad (137)$$

$$z' = C\alpha f_d R_o, \quad (138)$$

$$R_{xz}^2 = f_d^2 R_o^2, \quad (139)$$

$$R'_{xz}{}^2 = (C^2\beta S^2\alpha + C^2\alpha)f_d^2 R_o^2, \quad (140)$$

$$C\theta_{xz} = C\theta_{yz} = 1, \quad (141)$$

$$C\theta'_{xz} = \frac{C\alpha}{\sqrt{C^2\beta S^2\alpha + C^2\alpha}}, \quad (142)$$

$$C\theta'_{yz} = \frac{C\alpha}{\sqrt{S^2\beta S^2\alpha + C^2\alpha}}. \quad (143)$$

Using the above relationships, D_{rel} simplifies to

$$\begin{aligned} D_{rel} &= \frac{2C^2\alpha}{(C^2\beta S^2\alpha + C^2\alpha)^2 + (S^2\beta S^2\alpha + C^2\alpha)} \\ &= \frac{2}{1 + C^2\alpha + S^2\beta T^2\alpha + C^4\beta S^2\alpha T^2\alpha + 2C^2\beta S^2\alpha}. \end{aligned} \quad (144)$$

The equation for D_{rel} at 144 can be expressed in a Maclaurin series expansion in terms of α about $\alpha = 0$. Retaining only terms up to quadratic as usual, D_{rel} becomes

$$D_{rel} = 1 + \frac{(1 - 2C^2\beta - S^2\beta)\alpha^2}{2}. \quad (145)$$

Hence

$$\mu_{D_{rel}} = 1 - \frac{\sigma_a^2}{4}. \quad (146)$$

Then

$$(\mu_{D_{rel}})^2 \approx 1 - \frac{\sigma_a^2}{2}. \quad (147)$$

Similarly, a Maclaurin series expansion of D_{rel}^2 gives

$$D_{rel}^2 = 1 + (1 - 2C^2\beta - S^2\beta)\alpha^2 \quad (148)$$

from which

$$E[D_{rel}^2] = 1 - \frac{\sigma_a^2}{2} \quad (149)$$

so that

$$\sigma_{D_{rel}}^2 = E[D_{rel}^2] - (\mu_{D_{rel}})^2 = 0. \quad (150)$$

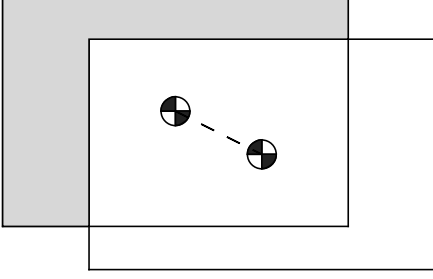


Figure 7: Field of View Erosion with Axis Error

Sampling Density Impact Interpretation In summary, for the optimal viewing geometry (zero inclination angle and measurements near the sensor boresight), $\mu_{D_{rel}}$ and $\sigma_{D_{rel}}^2$ are as follows:

$$\mu_{D_{rel}} = 1 - \frac{\sigma_a^2}{4}, \quad (151)$$

$$\sigma_{D_{rel}}^2 = 0. \quad (152)$$

Average sampling density is marginally reduced while the variance is zero. In the first case, benefits from the small but consistent range reduction are overpowered by the fact that all measurements under pose axis error at made slightly off boresight. As was the case for measurement precision, the variance of the sampling density is again zero due to the symmetrical viewing geometry under these conditions.

3.3.3 Visibility Impact

The visibility impact of sensor axis orientation error will depend on object shape, optical baseline length, sensor-object relative pose and the magnitude of the orientation error. Axis orientation error σ_a has the effect of causing a wobble in the position of the optical transmitter and receiver. The degree of wobble is determined by the orientation error, the length of the optical baseline and the position of the scan along the y-axis. Effects are similar to those generated by pose position error. Visibility impacts will generally be low at small axis orientation error σ_a .

3.3.4 Frustum Occupancy Impact

Field of View Erosion As illustrated in Figure 7, axis orientation error about the sensor boresight changes the sensor aiming point and thus potentially has a large impact on actual versus planned coverage.

At the specified stand-off range of $f_d R_o$, the projection of the sensor boresight on the frustum

cross-section is off-set by an amount $(d_x, d_y) = (f_d R_o T \alpha C \beta, f_d R_o T \alpha S \beta)$. Recall that we model axis error with two components, α and β . The off-boresight angle error α is modeled as a zero-mean Gaussian process with standard deviation σ_a while the angular location around the boresight β has a uniform distribution over $[-\pi, \pi]$. Then, the targeted sensor footprint is reduced to the following, where the scan length has again been optimally configured:

$$TF' = (2f_d R_o T \Phi_2 - |d_x|)(f_d R_o \Phi_x - |d_y|). \quad (153)$$

Then, the relative targeted footprint is

$$\begin{aligned} TF_{rel} &= \frac{(2f_d R_o T \Phi_2 - f_d R_o |T \alpha C \beta|)}{2f_d R_o T \Phi_2} \\ &= \frac{(f_d R_o \Phi_x - f_d R_o |T \alpha S \beta|)}{f_d R_o \Phi_x} \\ &= 1 - a|T \alpha C \beta| - b|T \alpha S \beta| \\ &\quad + cT^2 \alpha |C \beta S \beta| \end{aligned} \quad (154)$$

where $a = 1/2T\Phi_2$, $b = 1/\Phi_x$ and $c = 1/2T\Phi_2\Phi_x$.

Then the average relative targeted footprint is

$$\begin{aligned} \mu_{TF_{rel}} &= 1 - \sigma_a(a+b) \frac{2}{\pi} \sqrt{\frac{2}{\pi}} \\ &\quad + c \frac{\sigma_a^2}{\pi}. \end{aligned} \quad (155)$$

To compute the variance, we have

$$\begin{aligned} (\mu_{TF_{rel}})^2 &\approx 1 - \sigma_a(a+b) \frac{4}{\pi} \sqrt{\frac{2}{\pi}} \\ &\quad + 2c \frac{\sigma_a^2}{\pi} + \sigma_a^2(a+b)^2 \frac{8}{\pi^3}, \end{aligned} \quad (156)$$

$$\begin{aligned} E[TF_{rel}^2] &= 1 - \sigma_a(a+b) \frac{4}{\pi} \sqrt{\frac{2}{\pi}} + 2c \frac{\sigma_a^2}{\pi} \\ &\quad + 2ab \frac{\sigma_a^2}{\pi} + \frac{\sigma_a^2(a^2 + b^2)}{2}. \end{aligned} \quad (157)$$

Thus

$$\sigma_{TF_{rel}}^2 = \frac{\sigma_a^2}{2\pi^3} [(a^2 + b^2)(\pi^3 - 16) + 4ab(\pi^2 - 8)]. \quad (158)$$

In summary, the relative impact of the axis component of pose orientation error on field of view erosion is approximately

$$\mu T F_{rel} = 1 - \frac{(\Phi_x + 2T\Phi_2)}{\pi T\Phi_2\Phi_x} \sqrt{\frac{2}{\pi}} \sigma_a + \frac{\sigma_a^2}{2\pi T\Phi_2\Phi_x}, \quad (159)$$

$$\sigma T F_{rel}^2 = \frac{\sigma_a^2}{8\pi^3 T^2 \Phi_2 \Phi_x^2} [(4T^2\Phi_2 + \Phi_x^2)(\pi^3 - 16) + 8T\Phi_2\Phi_x(\pi^2 - 8)]. \quad (160)$$

The impact of the axis component of pose orientation error on viewpoint coverage calculated from Equations 159 and 160 is shown at Figure 10(d) for a line-scan sensor with $\Phi_x = 30^\circ$ and the optimum scanning geometry. One- and two-sigma curves for relative targeted footprint are displayed bracketing the average value. We observe that there is a high level of frustum erosion with pose axis orientation error and, hence a serious impact on view planning.

Depth of Field Erosion Pose error produces frustum erosion whenever $\delta_z > (f_d - 1)R_o$. Unlike the case of pose position error which results in catastrophic frustum erosion of an entire scan, frustum erosion under axis error is a slowly occurring phenomena, starting at the far edges of the frustum cross-section and gradually moving inward with increasing error.

It is easily shown that depth of field erosion from axis error will begin to occur in the yz-plane when

$$S\alpha > \frac{f_d - 1}{f_d\Phi_2} \quad (161)$$

and in the xz-plane when

$$S\alpha > \frac{f_d - 1}{\Phi_2}. \quad (162)$$

For small α , $S\alpha \approx \alpha$. Thus, using the most conservative test from 161 and 162, depth of field erosion will begin to occur for

$$\alpha > \frac{f_d - 1}{f_d\Phi_2}. \quad (163)$$

Therefore, the statistic of interest is the probability $P[\alpha > (f_d - 1)/(f_d\Phi_2)]$. Then,

$$P[\alpha > \frac{(f_d - 1)}{f_d\Phi_2}] = 1 - \Phi[\frac{(f_d - 1)}{f_d\Phi_2\sigma_a}]. \quad (164)$$

The probability of depth of field erosion with pose axis error is shown at Figure 8, plotted on a normalized logarithmic scale. These curves can be compared with

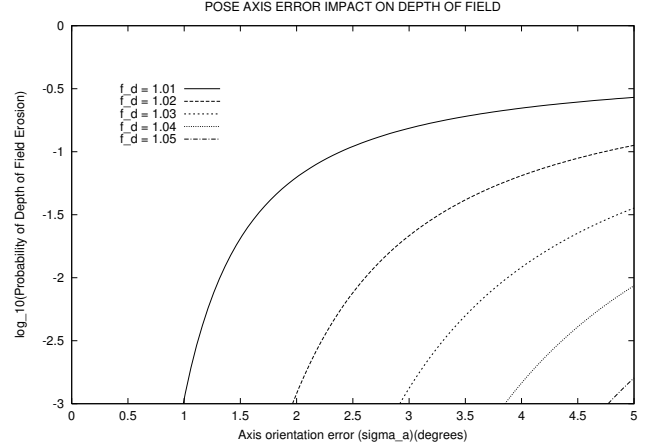


Figure 8: Axis Error Impact on Depth of Field

depth of field erosion with pose position error shown at Figure 10(b). Recall, however, that frustum depth of field erosion under axis error is gradual, whereas it is abrupt and catastrophic with position error. In summary, pose axis error results in only minor frustum depth of field erosion under most practical system configurations.

3.4 Twist Error

3.4.1 Measurement Precision Impact

Precision Estimation Model This section considers the effect of the twist component of pose orientation error on measurement precision estimation - that is, rotation error about the sensor boresight. Twist angle error α about the sensor z-axis is modeled as a zero-mean Gaussian process with standard deviation σ_t . The corresponding rotation matrix $R_{z,\alpha}$ is

$$R_{z,\alpha} = \begin{pmatrix} C\alpha & -S\alpha & 0 \\ S\alpha & C\alpha & 0 \\ 0 & 0 & 1 \end{pmatrix} \quad (165)$$

Range remains constant $z' = z = f_d R_o$, so the relative measurement precision P_{rel} is

$$P_{rel} = \frac{\hat{\sigma}_{z'}}{\hat{\sigma}_z} = \frac{\cos \theta_{yz}}{\cos \theta'_{yz}}. \quad (166)$$

Inclination angle θ_{yz} is the angle between the projection of the surface normal \vec{n} in camera space on the y-z plane $\vec{n}_{yz} = (0, n_y, n_z)$ and the camera boresight axis $\vec{u}_z = (0, 0, 1)$. Similarly, inclination angle

θ'_{yz} is the angle between the perturbed surface normal $\vec{n}_{yz}' = (0, n_y', n_z')$ and camera space $\vec{u}_{z'} = (0, 0, 1)$. Then,

$$C\theta_{yz} = \frac{\vec{n}_{yz} \cdot \vec{u}_z}{\|\vec{n}_{yz}\| \|\vec{u}_z\|} = \frac{n_z}{\sqrt{n_y^2 + n_z^2}}, \quad (167)$$

$$C\theta'_{yz} = \frac{\vec{n}_{yz}' \cdot \vec{u}_{z'}}{\|\vec{n}_{yz}'\| \|\vec{u}_{z'}\|} = \frac{n_z}{\sqrt{(S\alpha n_x + C\alpha n_y)^2 + n_z^2}}. \quad (168)$$

Consequently, as $n_x/n_z = T\theta_{xz}$ and $n_y/n_z = T\theta_{yz}$

$$\begin{aligned} \frac{\cos\theta_{yz}}{\cos\theta'_{yz}} &= \sqrt{\frac{(S\alpha n_x + C\alpha n_y)^2 + n_z^2}{n_y^2 + n_z^2}} \\ &= \sqrt{\frac{(S\alpha T\theta_{xz} + C\alpha T\theta_{yz})^2 + 1}{T^2\theta_{yz} + 1}} \\ &= C\theta_{yz} \sqrt{1 + (S\alpha T\theta_{xz} + C\alpha T\theta_{yz})^2}. \end{aligned} \quad (169)$$

Then, the relative measurement precision P_{rel} is

$$P_{rel} = C\theta_{yz} \sqrt{1 + (S\alpha T\theta_{xz} + C\alpha T\theta_{yz})^2}. \quad (170)$$

Statistics of P_{rel} Equation 170 can be rewritten as follows, where $a = (S\alpha T\theta_{xz} + C\alpha T\theta_{yz})^2$:

$$P_{rel} = C\theta_{yz} \sqrt{1 + a}. \quad (171)$$

As $T\theta_{xz} < \sqrt{3}$ and $T\theta_{yz} < \sqrt{3}$ in the range of interest and $\alpha \ll 1$, 171 can be approximated as

$$P_{rel} = C\theta_{yz} \left[1 + \frac{a}{2} - \frac{a^2}{8} + \frac{a^3}{16} - \frac{5a^4}{128} + \mathcal{O}(a^5) \right]. \quad (172)$$

Therefore, using Equations [115-125] and taking terms up to quadratic in σ_t , we get the following:

$$\begin{aligned} E[a] &= E[S^2\alpha T^2\theta_{xz} + C^2\alpha T^2\theta_{yz} \\ &\quad + 2S\alpha C\alpha T\theta_{xz}T\theta_{yz}] \\ &= \sigma_t^2 T^2\theta_{xz} + (1 - \sigma_t^2)T^2\theta_{yz}, \end{aligned} \quad (173)$$

$$E[a^2] = 6\sigma_t^2 T^2\theta_{xz}T^2\theta_{yz} + (1 - 2\sigma_t^2)T^4\theta_{yz}, \quad (174)$$

$$E[a^3] = 15\sigma_t^2 T^2\theta_{xz}T^4\theta_{yz} + (1 - 3\sigma_t^2)T^6\theta_{yz}, \quad (175)$$

$$E[a^4] = 28\sigma_t^2 T^2\theta_{xz}T^6\theta_{yz} + (1 - 4\sigma_t^2)T^8\theta_{yz}. \quad (176)$$

Collecting terms, we get

$$\begin{aligned} \mu_{P_{rel}} &= C\theta_{yz} \left[s_1 - \frac{\sigma_t^2 T^2\theta_{yz}}{2} s_2 \right. \\ &\quad \left. + \frac{\sigma_t^2 T^2\theta_{xz}}{2} s_3 \right] \end{aligned} \quad (177)$$

where

$$s_1 = 1 + \frac{1}{2}T^2 - \frac{1}{8}T^4 + \frac{1}{16}T^6 - \frac{5}{128}T^8 + \dots, \quad (178)$$

$$s_2 = 1 - \frac{1}{2}T^2 + \frac{3}{8}T^4 - \frac{5}{16}T^6 + \frac{35}{128}T^8 + \dots, \quad (179)$$

$$s_3 = 1 - \frac{3}{2}T^2 + \frac{15}{8}T^4 - \frac{35}{16}T^6 + \frac{315}{128}T^8 + \dots \quad (180)$$

and $T = T\theta_{yz}$. Closed form solutions exist for these infinite series, as follows:

$$s_1 = [1 + T^2]^{1/2} = \frac{1}{C\theta_{yz}}, \quad (181)$$

$$s_2 = [1 + T^2]^{-1/2} = C\theta_{yz}, \quad (182)$$

$$s_3 = [1 + T^2]^{-3/2} = C^3\theta_{yz}. \quad (183)$$

So the average relative precision is

$$\mu_{P_{rel}} = 1 + \frac{\sigma_t^2}{2} [T^2\theta_{xz}C^4\theta_{yz} - S^2\theta_{yz}]. \quad (184)$$

To calculate the variance, we compute

$$\begin{aligned} E[P_{rel}^2] &= E[C^2\theta_{yz}(1 + a)] \\ &= 1 + \sigma_t^2 T^2\theta_{xz}C^2\theta_{yz} - \\ &\quad \sigma_t^2 S^2\theta_{yz} \end{aligned} \quad (185)$$

$$\mu_{P_{rel}}^2 \approx 1 + \sigma_t^2 T^2\theta_{xz}C^4\theta_{yz} - \sigma_t^2 S^2\theta_{yz} \quad (186)$$

from which the variance of P_{rel} is

$$\sigma_{P_{rel}}^2 = \sigma_t^2 T^2\theta_{xz}S^2\theta_{yz}C^2\theta_{yz} \quad (187)$$

and the standard deviation is

$$\sigma_{P_{rel}} = \sigma_t T\theta_{xz}S\theta_{yz}C\theta_{yz}. \quad (188)$$

Precision Impact Interpretation Considering the behavior of relative precision P_{rel} for optimal scanning geometry of $\theta_{xz} = \theta_{yz} = 0$, we note from Equations 184 and 187 that its average is unchanged and variance is zero. These statistics result from the symmetrical viewing geometry under these special circumstances:

$$P_{rel} \approx 1, \quad (189)$$

$$\sigma P_{rel} \approx 0. \quad (190)$$

Even with non-optimal scanning geometry, it is evident that the effect of twist orientation error on precision estimation is marginal.

3.4.2 Sampling Density Impact

Sampling Density Estimation Model This section considers the effect of the twist component of pose orientation error on sampling density estimation. From Equation 12, our model for relative sampling density D_{rel} is

$$D_{rel} = \frac{C^2 \theta'_{xz} C^2 \theta'_{yz} R_{xz}^2 C^2 \theta_{yz} + f_d^2 R_o^2 C^2 \theta_{xz}}{C^2 \theta_{xz} C^2 \theta_{yz} R'_{xz}{}^2 C^2 \theta'_{yz} + f_d^2 R_o^2 C^2 \theta'_{xz}}. \quad (191)$$

For rotation error angle α about the boresight, we have the following geometric relationships

$$R_{xz}^2 = z^2 + x^2 = f_d^2 R_o^2 + x^2, \quad (192)$$

$$R'_{xz}{}^2 = z'^2 + x'^2, \quad (193)$$

$$z' = z = f_d R_o, \quad (194)$$

$$x' = C\alpha x - S\alpha y, \quad (195)$$

$$C^2 \theta_{xz} = \frac{n_z^2}{n_x^2 + n_z^2}, \quad (196)$$

$$C^2 \theta_{yz} = \frac{n_z^2}{n_y^2 + n_z^2}, \quad (197)$$

$$C^2 \theta'_{xz} = \frac{n_z^2}{(C\alpha n_x - S\alpha n_y)^2 + n_z^2}, \quad (198)$$

$$C^2 \theta'_{yz} = \frac{n_z^2}{(S\alpha n_x + C\alpha n_y)^2 + n_z^2}. \quad (199)$$

From the above, 191 reduces to

$$\begin{aligned} D_{rel} &= \frac{(1 + x_r^2)(1 + T^2 \theta_{xz}) + (1 + T^2 \theta_{yz})}{(1 + t1^2)(1 + t2^2) + (1 + t3^2)} \\ &= \frac{N}{D} \end{aligned} \quad (200)$$

where $x_r = x/f_d R_o = \tan \phi_{xz}$, $y_r = y/f_d R_o$, $t1 = C\alpha x_r - S\alpha y_r$, $t2 = C\alpha T\theta_{xz} - S\alpha T\theta_{yz}$, and $t3 = S\alpha T\theta_{xz} + C\alpha T\theta_{yz}$.

The numerator of 200 reduces to

$$\begin{aligned} N &= \frac{(1 + x_r^2)C^2 \theta_{yz} + C^2 \theta_{xz}}{C^2 \theta_{xz} C^2 \theta_{yz}} \\ &= \frac{C^2 \theta_{yz} + C^2 \phi_{xz} C^2 \theta_{yz}}{C^2 \theta_{yz} C^2 \phi_{xz} C^2 \theta_{yz}}. \end{aligned} \quad (201)$$

As $|t1|$, $|t2|$ and $|t3|$ are all < 1 over the range of interest, the denominator can be written as $D = 2(1 + t)$ where $t = (t1^2 + t2^2 + t3^2 + t1^2 t2^2)/2$. Then, the relative sampling density D_{rel} is

$$D_{rel} = \frac{N}{2(1 + t)} \quad (202)$$

which can be further written as

$$D_{rel} = \frac{N}{2}(1 - t + \mathcal{O}(t^2)). \quad (203)$$

Statistics of D_{rel} Considering only terms up to quadratic in the key variables, the average relative sampling density $\mu_{D_{rel}}$ is approximately

$$\mu_{D_{rel}} = E\left[\frac{N}{2}(1 - t)\right] \quad (204)$$

where

$$E[t] = \frac{1}{2}\{E[t1^2] + E[t2^2] + E[t3^2] + E[t1^2]E[t2^2]\}, \quad (205)$$

$$\begin{aligned} E[t1^2] &= E[C^2 \alpha x_r^2 + S^2 \alpha y_r^2 - 2S\alpha C\alpha x_r y_r] \\ &= (1 - \sigma_t^2)x_r^2 + \sigma_t^2 y_r^2, \end{aligned} \quad (206)$$

$$\begin{aligned} E[t2^2] &= E[C^2 \alpha T^2 \theta_{xz} + S^2 \alpha T^2 \theta_{yz} \\ &\quad - 2S\alpha C\alpha T\theta_{xz} T\theta_{yz}] \\ &= (1 - \sigma_t^2)T^2 \theta_{xz} + \sigma_t^2 T^2 \theta_{yz}, \end{aligned} \quad (207)$$

$$\begin{aligned}
E[t^3] &= E[S^2\alpha T^2\theta_{xz} + C^2\alpha T^2\theta_{yz} \\
&\quad + 2S\alpha C\alpha T\theta_{xz}T\theta_{yz}] \\
&= \sigma_t^2 T^2\theta_{xz} + (1 - \sigma_t^2)T^2\theta_{yz}, \quad (208)
\end{aligned}$$

$$\begin{aligned}
E[t^2t^2] &= E[(C^2\alpha x_r^2 + S^2\alpha y_r^2 - 2S\alpha C\alpha x_r y_r) \\
&\quad (C^2\alpha T^2\theta_{xz} + S^2\alpha T^2\theta_{yz} \\
&\quad - 2S\alpha C\alpha T\theta_{xz}T\theta_{yz})] \\
&= (1 - 2\sigma_t^2)x_r^2 T^2\theta_{xz} + \sigma_t^2 y_r^2 T^2\theta_{xz} \\
&\quad + \sigma_t^2 x_r^2 T^2\theta_{yz} + 4\sigma_t^2 x_r y_r T\theta_{xz}T\theta_{yz}, \quad (209)
\end{aligned}$$

$$\begin{aligned}
E[t] &= \frac{1}{2}\{x_r^2(1 + T^2\theta_{xz}) + T^2\theta_{xz} + T^2\theta_{yz} + \\
&\quad \sigma_t^2[-x_r^2(1 + 2T^2\theta_{xz}) + y_r^2(1 + T^2\theta_{xz}) + \\
&\quad x_r^2 T^2\theta_{yz} + 4x_r y_r T\theta_{xz}T\theta_{yz}]\}. \quad (210)
\end{aligned}$$

Collecting terms, we get the following expression for the average relative sampling density $\mu_{D_{rel}}$ where N is defined at 201:

$$\begin{aligned}
\mu_{D_{rel}} &\approx \frac{N}{4}[2 - x_r^2(1 + T^2\theta_{xz}) - T^2\theta_{xz} - T^2\theta_{yz}] \\
&\quad + \frac{\sigma_t^2 N}{4}[x_r^2(1 + 2T^2\theta_{xz}) \\
&\quad - y_r^2(1 + T^2\theta_{xz}) - x_r^2 T^2\theta_{yz} \\
&\quad - 4x_r y_r T\theta_{xz}T\theta_{yz}]. \quad (211)
\end{aligned}$$

For the variance, we have the following, considering terms to $\mathcal{O}(t^2)$

$$\mu_{D_{rel}} \approx \frac{N}{2}(1 - E[t] + E[t^2]), \quad (212)$$

$$\mu_{D_{rel}}^2 \approx \frac{N^2}{4}(1 - 2E[t] + (E[t])^2 + 2E[t^2]), \quad (213)$$

$$E[D_{rel}^2] = \frac{N^2}{4}(1 - 2E[t] + 3E[t^2]). \quad (214)$$

Therefore, the variance $\sigma_{D_{rel}}^2$ is

$$\begin{aligned}
\sigma_{D_{rel}}^2 &\approx \frac{N^2}{4}(E[t^2] - (E[t])^2) \\
&= \frac{N^2\sigma_t^2 x_r^2}{4}[y_r(1 + T^2\theta_{xz}) \\
&\quad + x_r T\theta_{xz}T\theta_{yz}]^2. \quad (215)
\end{aligned}$$

Hence, the standard deviation $\sigma_{D_{rel}}$ is

$$\begin{aligned}
\sigma_{D_{rel}} &\approx \frac{N\sigma_t x_r}{2}[y_r(1 + T^2\theta_{xz}) \\
&\quad + x_r T\theta_{xz}T\theta_{yz}]. \quad (216)
\end{aligned}$$

Sampling Density Impact Interpretation Considering the behavior of relative sampling density for optimal scanning geometry of $\theta_{xz} = \theta_{yz} = 0$, the coefficient N reduces to $(1 + C^2\phi_{xz})/C^2\phi_{xz}$ and we obtain the following simplified expressions for the average and variance of D_{rel} from Equations 211 and 216:

$$\mu_{D_{rel}} \approx \frac{N}{4}[2 - x_r^2] + \frac{\sigma_t^2 N}{4}[x_r^2 - y_r^2], \quad (217)$$

$$\sigma_{D_{rel}} \approx \frac{N\sigma_t x_r y_r}{2}. \quad (218)$$

Furthermore, for measurements near the sensor boresight ($x_r \approx 0 \approx y_r$), then

$$\mu_{D_{rel}} \approx 1, \quad (219)$$

$$\sigma_{D_{rel}} \approx 0. \quad (220)$$

Even with non-optimal scanning geometry, it is evident that the effect of twist orientation error on sampling density estimation is marginal.

3.4.3 Visibility Impact

The visibility impact of sensor twist orientation error will depend on the object shape, sensor optical baseline, sensor-object relative pose and the magnitude of the orientation error. Visibility impacts will generally be low at small twist orientation error σ_t . However, occasionally even small orientation errors may be sufficient to push the visibility of surface elements near threshold into occlusion. Moderate to large twist orientation errors will result in significant unplanned occlusions due to shadow effects arising from the non-zero optical baseline.

3.4.4 Frustum Occupancy Impact

Field of View Erosion As illustrated in Figure 9, twist orientation error about the sensor boresight reduces the effective coverage. It is readily shown that coverage reduction δ_{TF} is as follows, where W and L are the width and length of the frustum cross-section at the desired stand-off range:

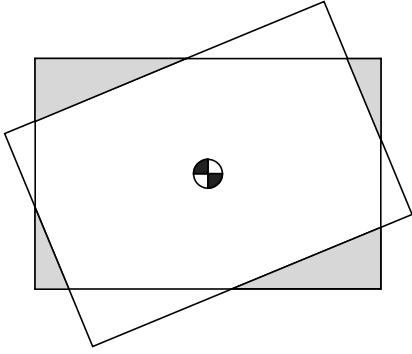


Figure 9: Field of View Erosion with Twist Error

$$\delta_{TF} = \frac{1 - C\alpha}{2|S\alpha|C\alpha} [L^2 + W^2 - 2LW|S\alpha|]. \quad (221)$$

As we are interested only in relatively small angle errors, the absolute value operator need only be applied to the $S\alpha$ term. It is convenient to rewrite the foregoing as

$$\delta_{TF} = \frac{LW(C\alpha - 1)}{C\alpha} + \frac{|S\alpha|(L^2 + W^2)}{2C\alpha(1 + C\alpha)}. \quad (222)$$

For small α and considering only terms up to quadratic, Equation 222 can be approximated by the following:

$$\delta_{TF} \approx -\frac{LW\alpha^2}{2} + \frac{|\alpha|(L^2 + W^2)}{4}. \quad (223)$$

Consequently, the relative targeted footprint is

$$\begin{aligned} TF_{rel} &= \frac{LW - \delta_{TF}}{LW} \\ &= 1 - \frac{|\alpha|(L^2 + W^2)}{4LW} + \frac{\alpha^2}{2}. \end{aligned} \quad (224)$$

As the frustum width at the optimum stand-off range is $W = 2f_d R_o T \Phi_2$ and the scan length has been optimized to $L = f_d R_o \Phi_x$, 224 is

$$TF_{rel} = 1 - a|\alpha| + \frac{\alpha^2}{2} \quad (225)$$

where

$$a = \frac{\Phi_x^2 + 4T^2\Phi_2}{8\Phi_x T \Phi_2}. \quad (226)$$

Then, the average relative targeted footprint is

$$\mu_{TF_{rel}} = 1 - a\sigma_t \sqrt{\frac{2}{\pi}} + \frac{\sigma_t^2}{2}. \quad (227)$$

Similarly,

$$E[TF_{rel}^2] = 1 - 2a\sigma_t \sqrt{\frac{2}{\pi}} + (a^2 + 1)\sigma_t^2. \quad (228)$$

Consequently, the variance $\sigma_{TF_{rel}}$ is

$$\begin{aligned} \sigma_{TF_{rel}}^2 &= E[TF_{rel}^2] - (\mu_{TF_{rel}})^2 \\ &= a^2\sigma_t^2 \frac{(\pi - 2)}{\pi}. \end{aligned} \quad (229)$$

In summary, the relative impact of the twist component of viewpoint orientation error on field of view erosion is approximately

$$\mu_{TF_{rel}} = 1 - \frac{\Phi_x^2 + 4T^2\Phi_2}{8\Phi_x T \Phi_2} \sqrt{\frac{2}{\pi}} \sigma_t + \frac{\sigma_t^2}{2}, \quad (230)$$

$$\sigma_{TF_{rel}} = \frac{\Phi_x^2 + 4T^2\Phi_2}{8\Phi_x T \Phi_2} \sqrt{\frac{\pi - 2}{\pi}} \sigma_t. \quad (231)$$

The impact of the twist component of pose orientation error on viewpoint coverage calculated from Equations 230 and 231 is shown at Figure 10(f) for a line-scan sensor with $\Phi_x = 30^\circ$. One- and two-sigma curves for relative targeted footprint are displayed bracketing the average value. We observe that pose twist orientation error results in low frustum erosion and thus impacts view planning.

Depth of Field Erosion As twist orientation error does not change the sensor stand-off range, it does not erode the sensor depth of field.

4 Summary and Conclusions

4.1 Overview

Table 2 provides a qualitative overview of pose error effects on a single view. On a relative basis, effects are broadly categorized in the range: high (H), moderate (M), low (L) or nil. Analytical results in pose error variables up to second order effects are presented at Tables 3 and 4. Error effects with non-zero variance

	Position	Axis	Twist
Measurement Precision	L-M	L	nil
Sampling Density	L-M	L	nil
Visibility	L	L	M
Frustum Occupancy	M-H	H	L

Table 2: Qualitative Pose Error Effects

are plotted at Figure 10, allowing a quantitative comparison. Table 6 summarizes key symbols and definitions.

The effects of pose position and pose orientation error are shown. The latter is broken down into sensor boresight axis error and rotation error about the sensor boresight (twist). In all cases, performance is relative to the error-free case.

Finally, note that the foregoing results are based on an optimized scanning configuration of a line-scan range camera, the conditions for which are summarized at Table 5. Results for non-optimized scanning configurations can be found in the appropriate subsections to Section 3.

4.2 Pose Error Model Suitability

This analysis has employed a simple, general purpose error model based on Gaussian statistics. The statistical behavior of real positioning systems is more complex and highly variable between system type and configuration. Pose error is also very difficult to characterize and quantify in practice. Furthermore, each type of pose error effect has been studied in isolation. Multiple types of pose error in combination will interact in a non-linear manner. Nevertheless, while its limitations are acknowledged, the pose error model employed here should form a suitable basis for understanding pose error effects and in selecting countermeasures to deal with them.

4.3 Measurement Performance

The effects of pose error on measurement performance (precision and sampling density) for a single viewpoint are summarized at Table 3. Average measurement performance is only slightly effected by second order effects which will be small in most practical cases.

In the case of position error, average relative measurement precision is slightly degraded due to the quadratic variation of sensor precision with range. On the other hand, average relative sampling density is slightly improved as the improvement at shorter

ranges slightly outweighs degradation at longer ranges. However, the important statistic is measurement variance which is low to moderate. Unless taken into account, pose position error will degrade view planning performance.

For axis orientation error, average relative measurement precision is marginally improved as range to the target is reduced. Average relative sampling density is slightly degraded by off-boresight and inclination angle effects. Measurement variance is zero as a result of symmetry. Thus, the net effect of axis orientation error on measurement performance is low.

For twist orientation error, both average relative measurement precision and average relative sampling density are unchanged and the measurement variance is zero due to symmetry. Considered in isolation, twist orientation error has negligible effect on measurement performance. However, note comments under visibility.

4.4 Visibility

Visibility or occlusion effects depend on several variables, only a few of which are restricted to the sensor or positioning system. The most important sensor parameter is the length of the optical baseline. Fixed for any given sensor, this parameter directly influences measurement performance, shadow effects and the ability to observe the interior of cavities. It is important to select a range camera with an optical baseline appropriate to the modeling task.

Two other major factors impacting visibility are object shape and relative sensor-object pose. The former cannot be altered and varies from task to task. Selecting appropriate sensor poses is the essence of view planning.

Once a pose has been generated, selected and included in the next-best-view list, pose error induced by the positioning system will influence actual visibility. In the case of pose position error, the visibility impact will be low to nil. The exception could be the case of surface regions being viewed at incidence angles near threshold or close to occlusion. This effect can be reduced by using conservative visibility tests in measurability calculations.

Axis orientation error has the effect of causing a wobble in the position of the optical transmitter and receiver. The degree of wobble is determined by the orientation error, the length of the optical baseline and the position of the scan along the y-axis. Effects are similar to those generated by pose position error. Visibility impacts will generally be low for small axis orientation error.

On the other hand, twist orientation error has the potential to significantly degrade the reliability of visibility predictions as it results in leveraged movement of the laser source and optical detector in a plane tangential to the targeted object region. Very small twist errors will have a minor impact in most imaging situations. However, moderate twist error can introduce significant occlusion problems with convoluted object shapes. This is also the reason why optimizing the twist component of pose is so important during generation of candidate viewpoints.

4.5 Sensor Coverage

The third component of pose error is its effect on sensor coverage. This is particularly problematic as the whole point of view planning is to generate an optimal set of NBVs with specific coverage and measurability. If actual viewpoint coverage is significantly altered, the entire view planning process is undermined and can be rendered futile.

Pose error erodes the reliable coverage zone i.e. the field of view and depth of view. The effects of pose error on field of view erosion for a single viewpoint are summarized at Table 4. Recall that Φ_x is the sensor field of view in the x-z plane and $\Phi_2 = \Phi_x/2$. Field of view erosion effects are shown at Figure 10(e),(d) and (f) for pose position, axis and twist error, respectively. From these curves, we observe that all three error components have a non-negligible impact on sensor coverage. We can characterize the effects as low for twist error, high for axis error and moderate-to-high for position error. As expected, axis error is particularly troublesome as the abbe effect amplifies coverage perturbations with standoff range.

Some depth-of-field erosion occurs with pose position error. This is easily dealt with by a careful choice of the stand-off distance factor f_d . Depth-of-field erosion is negligible for pose orientation error.

4.6 Multiple Views

While the focus of this paper is on the effect of pose error on a single view, it is appropriate to briefly address the ramifications of pose error on view plans consisting of multiple views.

In most practical imaging situations, multiple view plans involve a great deal of redundant coverage for a variety of reasons:

- *Shape-driven image overlap* - The more complex the geometry, the greater the number of views required to capture the shape. This naturally leads

to considerable image overlap around regions of high shape complexity.

- *Image-based registration overlap* - Pose uncertainty sufficiently large to require image-based registration inherently requires image overlap and therefore builds in redundancy.
- *Non-optimal set covering algorithms* - The set covering problem is known to be NP-complete [16]. Thus, any practical set covering algorithm is sub-optimal, resulting in a view plan longer than the theoretical lower bound. Longer view plans equate to redundancy. Ironically, efficient view plans are more vulnerable to pose error effects.
- *Coverage gain from pose error* - This analysis has focussed on coverage loss due to pose error with a single view. However, where there is loss, there is gain. With multiple views, some coverage gain may partially off-set coverage losses.

The advantage of the redundancy phenomena is that it can mask most effects of low levels of pose error in some cases. The phenomena is not amenable to easy analytical treatment due to the large role played by object shape and the fact that NBV sets are typically small, such that composite coverage statistics are not well behaved. Initial experimental results with multiple view sets show partial-to-complete masking of pose error effects at low pose error levels, followed by a rapid decrease in average coverage and rapid increase in coverage variance as pose error further deteriorates.

The hidden problem with redundancy is that coverage results can be quite unpredictable. As the penalty for coverage failure is typically high for object reconstruction tasks³, the coverage unpredictability of pose error on multiple view sets can be unacceptable.

4.7 Pose Error Countermeasures

A variety of countermeasures are available to deal with positioning system error. The quantitative analysis of this paper may assist in setting key parameters.

- *Avoid the problem* - Pose error effects are sufficiently deleterious that they are best avoided by using the highest quality positioning system affordable. A CMM or other high accuracy positioning system avoids many problems.

³The imaging team may have left the site or the object may no longer be readily available by the time coverage gaps or measurability deficiencies are discovered.

- *Compatible system design* - The specification and design of an object reconstruction system should treat the camera and positioning system as equally important components of an integrated system. Trade-offs in one impact the other.
- *System modeling and calibration* - Both the range camera and positioning system must be regularly calibrated. Good quality system models are essential and parameters should be updated after each calibration.
- *Optimize standoff range selection* - The standoff range can be selected to avoid depth of field erosion while optimizing measurement performance.
- *Detune viewpoint generation* - Detuning the physical dimensions of the sensor frustum during measurability calculations decreases the probability of measurability or coverage failure.
- *Add image-based registration constraint [16]* - This has similar effects to frustum detuning. The two constraints can be combined.
- *Use conservative viewpoint testing* - Make viewpoint testing tolerant with respect to pose error effects on occlusion and proximity to incidence angle thresholds.
- *Feed back control loop* - Most positioning systems are open loop - that is, they are commanded to move to a specific pose and there is no control mechanism to confirm the fidelity with which the command was executed. It may be appropriate to consider a closed loop control system to reduce residual pose errors, perhaps through the use of machine vision or photogrammetric adjuncts to the positioning system.

Many of the foregoing countermeasures result in lengthened view plans. This has associated costs in scanning, registration and integration time and resources. Consequently, there are further trade-offs to be made between all phases of the object reconstruction process.

4.8 Conclusions

Performance-oriented view planning commences with a model specification requiring views (range images) to pass specific criteria for sampling precision and density, visibility and frustum occupancy. Unfortunately, positioning system errors negatively impact all of these requirements, with the severity generally

being in the order of frustum occupancy, measurement variation and occlusion. Additionally, pose error imposes image-based registration constraints on view plan generation. In turn, this increases the length of the view plan and the time span of all associated model reconstruction steps. Finally, collision avoidance planning is exacerbated by pose uncertainty.

Consequently, during view planning, we need to take both sensor and positioning system error models into account. It is clearly pointless to attempt subtle view planning optimization beyond the precision of the positioning system. This paper has provided a qualitative and quantitative analysis of pose error effects on a common type of range camera. Based on this analysis, countermeasures have been identified to mitigate pose error effects on object reconstruction.

References

- [1] J. E. Banta and M. A. Abidi. The positioning of a range sensor for optimal reconstruction of three-dimensional models. In *Int. Conf. on Recent Advances in 3D Digital Imaging and Modeling, Ottawa*, May 12-15 1997.
- [2] P. J. Besl. Range image sensors. In J. Sanz, editor, *Advances in Machine Vision*. Springer-Verlag, New York, 1989.
- [3] P. J. Besl and H. D. McKay. A method for registration of 3D shapes. *IEEE Trans. PAMI*, 14(2):239–256, February 1992.
- [4] P. Cauchick-Miguel, T. King, and J. Davis. CMM verification: A survey. *Measurement*, 17(1):1–16, 1996.
- [5] C. Connolly. The determination of next best views. In *Proc. IEEE Int. Conf. on Robotics and Automation*, pages 432–435, 1985.
- [6] K. Fu, R. Gonzalez, and C. Lee. *Robotics: Control, Sensing, Vision and Intelligence*. McGraw-Hill, 1987.
- [7] D. Lamb, D. Baird, and M. Greenspan. An automation system for industrial 3D laser digitizing. In *Second Int. Conf. on 3D Digital Imaging and Modeling, Ottawa*, pages 148–157, October 4-8 1999.
- [8] N. A. Massios and R. B. Fisher. A best next view selection algorithm incorporating a quality criterion. In *British Machine Vision Conference 1998*, pages 780–789, September, 1998.
- [9] J. Maver and R. Bajcsy. Occlusions as a guide for planning the next view. *IEEE Trans. PAMI*, 17(5):417–433, May 1993.
- [10] Newport. Motion control catalogue. Technical report, www.newport.com, 2000.

- [11] D. Papadopoulos-Orfanos and F. Schmitt. Automatic 3D digitization using a laser rangefinder with a small field of view. In *Int. Conf. on Recent Advances in 3D Digital Imaging and Modeling, Ottawa*, pages 60–67, May 12-15 1997.
- [12] R. Pito. A sensor based solution to the next-best-view problem. In *Proc. Int. Conf. on Pattern Recognition*, pages 941–945, August 1996.
- [13] C. J. Pudney. *Surface Modelling and Surface Following for Robots Equipped with Range Sensors*. PhD thesis, Univ. of Western Australia, Perth, 1994.
- [14] M. Reed, P. Allen, and I. Stamos. Automated model acquisition from range images with view planning. In *Proc. IEEE Conf. Vis. Pat. Rec., San Juan, Puerto Rico*, pages 72–77, June 17-19 1997.
- [15] W. Scott, G. Roth, and J.-F. Rivest. Performance-oriented view planning for automatic model acquisition. In *31st Int. Symposium on Robotics, Montreal*, pages 314–319, May 2000.
- [16] W. Scott, G. Roth, and J.-F. Rivest. View planning as a set covering problem. Technical Report ERB-1089, NRC-44889, National Research Council of Canada (NRCC), Institute for Information Technology, 2001.
- [17] W. Scott, G. Roth, and J.-F. Rivest. View planning for multi-stage object reconstruction. In *14th Int. Conf. on Vision Interface, Ottawa*, pages 64–71, 2001.
- [18] W. Scott, G. Roth, and J.-F. Rivest. View planning with a registration constraint. In *Third Int. Conf. on 3D Digital Imaging and Modeling, Quebec City, Canada*, pages 127–134, 2001.
- [19] Y. Shin and Y. Wei. A statistical analysis of positional errors of a multi-axis machine tool. *Precision Engineering*, 14(3):139–146, July 1992.
- [20] J. Soons, F. Thomas, and P. Schellekens. Modeling the errors of multi-axis machines: A general methodology. *Precision Engineering*, 14(1):5–19, July 1992.
- [21] I. Stamos and P. Allen. Interactive sensor planning. In *Proc. IEEE Conf. Vis. Pat. Rec., Santa Barbara, CA*, pages 489–494, June 23-25 1998.
- [22] G. Tarbox and S. Gottschlich. Planning for complete sensor coverage in inspection. *Computer Vision and Image Understanding*, 61(1):84–111, January 1995.
- [23] P. Whaite and F. P. Ferrie. Autonomous exploration: Driven by uncertainty. *IEEE Trans. PAMI*, 19(3):193–205, March 1997.
- [24] X. Yuan. A mechanism of automatic 3D object modeling. *IEEE Trans. PAMI*, 17(3):307–311, March 1995.

Measurement	Pose Position Error	Pose Axis Error	Pose Twist Error
Precision	$\mu_{P_{rel}} = 1 + \frac{1}{3f_d^2} \frac{\sigma_p^2}{R_o^2}$ $\sigma_{P_{rel}}^2 = \frac{4}{3f_d^2} \frac{\sigma_p^2}{R_o^2}$	$\mu_{P_{rel}} = 1 - \frac{3\sigma_a^2}{4}$ $\sigma_{P_{rel}}^2 = 0$	$\mu_{P_{rel}} = 1$ $\sigma_{P_{rel}}^2 = 0$
Sampling Density	$\mu_{D_{rel}} = 1 + \frac{1}{3f_d^2} \frac{\sigma_p^2}{R_o^2}$ $\sigma_{D_{rel}}^2 = \frac{2}{3f_d^2} \frac{\sigma_p^2}{R_o^2}$	$\mu_{D_{rel}} = 1 - \frac{\sigma_a^2}{4}$ $\sigma_{D_{rel}}^2 = 0$	$\mu_{D_{rel}} = 1$ $\sigma_{D_{rel}}^2 = 0$

Table 3: Single View Pose Error Measurability Effects: Line-scan Sensor

Error	Field of View Erosion	Depth of Field Erosion
Position	$\mu_{TF_{rel}} = 1 - \frac{(\Phi_x T \Phi_2 + \Phi_x + 2T \Phi_2)}{2f_d \Phi_x T \Phi_2} \sqrt{\frac{2}{3\pi}} \frac{\sigma_p}{R_o} + \frac{(T \Phi_2 + 1)}{3\pi f_d^2 \Phi_x T \Phi_2} \frac{\sigma_p^2}{R_o^2}$ $\sigma_{TF_{rel}}^2 = \frac{(\Phi_x T \Phi_2 + \Phi_x + 2T \Phi_2)^2}{4f_d^2 \Phi_x^2 T^2 \Phi_2} \left(\frac{\pi - 2}{3\pi} \right) \frac{\sigma_p^2}{R_o^2}$	$P[p_z > (f_d - 1)R_o] = 1 - \Phi\left[\frac{\sqrt{3}(f_d - 1)}{\sigma_p/R_o}\right]$
Axis	$\mu_{TF_{rel}} = 1 - \frac{(\Phi_x + 2T \Phi_2)}{\pi T \Phi_2 \Phi_x} \sqrt{\frac{2}{\pi}} \sigma_a + \frac{\sigma_a^2}{2\pi T \Phi_2 \Phi_x}$ $\sigma_{TF_{rel}}^2 = \frac{\sigma_a^2}{8\pi^3 T^2 \Phi_2 \Phi_x^2} [(4T^2 \Phi_2 + \Phi_x^2)(\pi^3 - 16) + 8T \Phi_2 \Phi_x (\pi^2 - 8)]$	$P[\alpha > \frac{(f_d - 1)}{f_d \Phi_2}] = 1 - \Phi\left[\frac{(f_d - 1)}{f_d \Phi_2 \sigma_a}\right]$
Twist	$\mu_{TF_{rel}} = 1 - \frac{\Phi_x^2 + 4T^2 \Phi_2}{8\Phi_x T \Phi_2} \sqrt{\frac{2}{\pi}} \sigma_t + \frac{\sigma_t^2}{2}$ $\sigma_{TF_{rel}}^2 = \frac{(\Phi_x^2 + 4T^2 \Phi_2)^2}{64\Phi_x^2 T^2 \Phi_2} \left(\frac{\pi - 2}{\pi} \right) \sigma_t^2$	nil

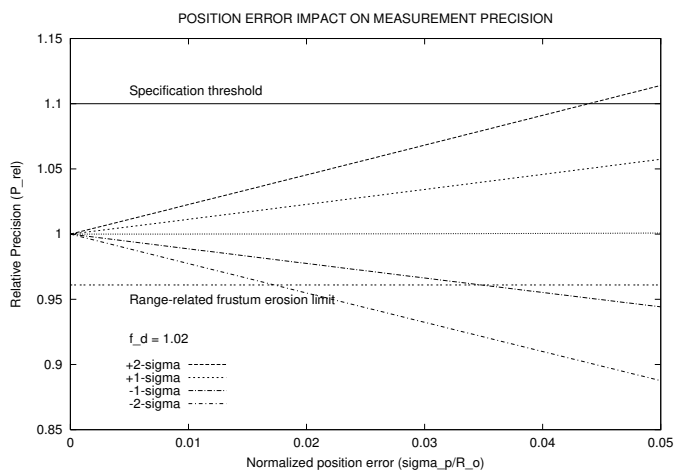
Table 4: Single View Pose Error Coverage Effects: Line-scan Sensor

	Condition
1	Symmetric image: $N_x = N_y = N$
2	Scan length optimized for even sampling in x and y: $L_y = f_d R_o \Phi_x$
3	Optimal stand-off distance: $z = f_d R_o$
4	Measurements normal to the surface: $\theta_{xz} = \theta_{yz} = 0$
5	Measurements near sensor boresight: $\phi_{xz} = 0, x = y = 0$

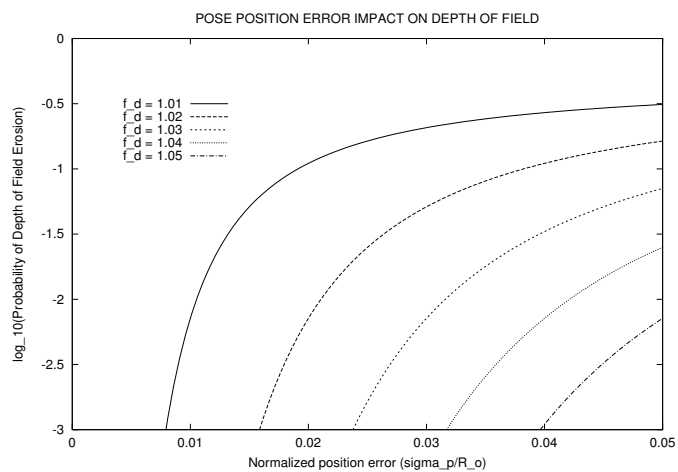
Table 5: Optimal Scanning Conditions: Line-scan Sensor

Symbol	Definition
P_{rel}	Relative measurement precision (error vs. error-free)
D_{rel}	Relative sampling density (error vs. error-free)
TF_{rel}	Relative targeted footprint (error vs. error-free)
σ_p	Pose position uncertainty standard deviation
σ_a	Pose axis angle uncertainty standard deviation
σ_t	Pose twist angle uncertainty standard deviation
R_o	Optimum sensor scanning range
f_d	Sensor standoff distance factor $f_d = 1 + \delta$, $\delta \ll 1$
Φ_x	Sensor field of view in the scanning plane
Φ_2	$\Phi_2 = \Phi_x/2$
$T\Phi_2$	$\tan \Phi_2$
L_y	Sensor linear scan length along y-axis
N_x, N_y	Number of range image samples in x- and y-axes
ϕ_{xz}	Scan angle in sensor xz-plane
θ_{xz}, θ_{yz}	Laser scanning ray incidence angles in xz- and yz-planes
p_x, p_y, p_z	Pose position error in x-, y- and z-axes
α	Pose axis error cone half-angle
$\Phi[z]$	Normal distribution function $\Phi[z] = \frac{1}{\sqrt{2\pi}} \int_{-\infty}^z e^{-u^2/2} du$

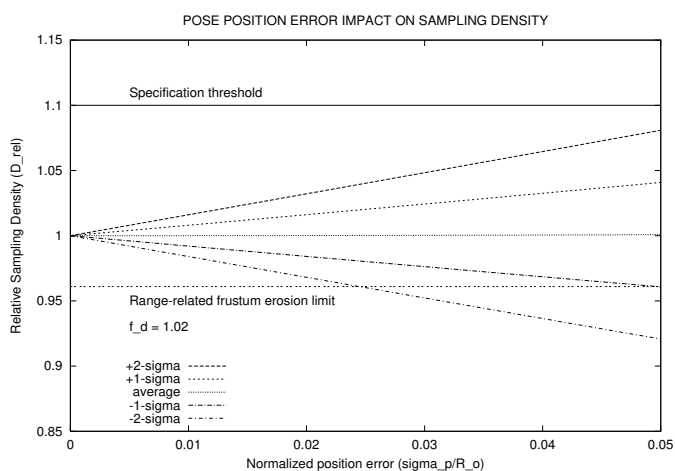
Table 6: Key Symbols and Definitions



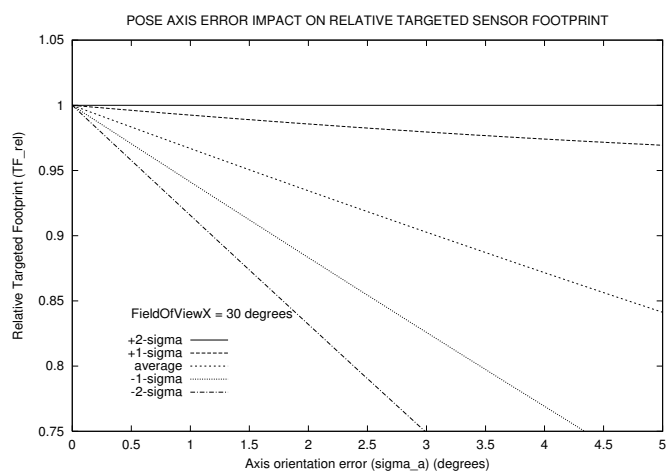
(a)



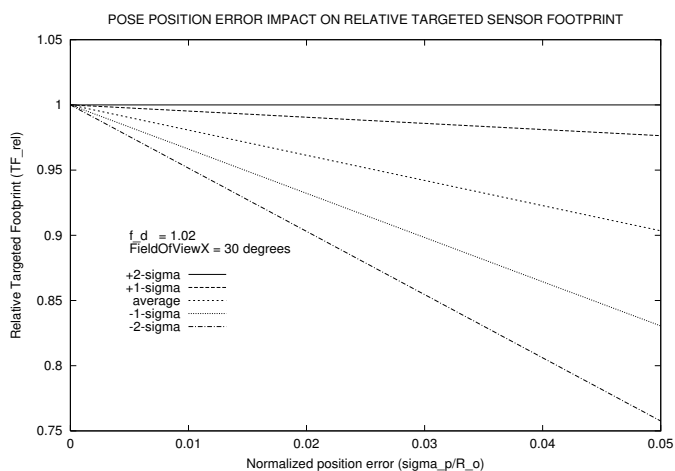
(b)



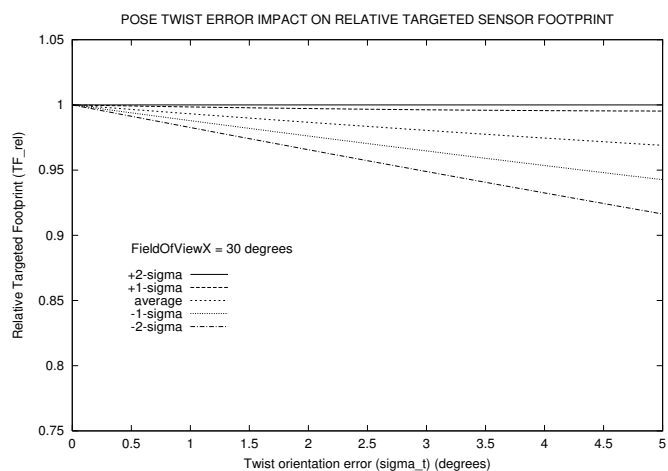
(c)



(d)



(e)



(f)

Position error - precision, density, FOV

Position error - DOF; Axis error - FOV; Twist error - FOV

Figure 10: Pose Error Effects